Ecological Engineering 180 (2022) 106676

Contents lists available at ScienceDirect

Ecological Engineering

journal homepage: www.elsevier.com/locate/ecoleng

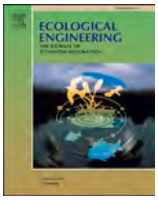

Development of a morphometric connectivity model to mitigate sediment derived from storm-driven shallow landslides

Raphael I. Spiekermann [a,b,*], Hugh G. Smith [a], Sam McColl [b], Lucy Burkitt [b], Ian C. Fuller [b]

[a] Manaaki Whenua – Landcare Research, Palmerston North, New Zealand
[b] School of Agriculture and Environment, Massey University, Palmerston North, New Zealand

ARTICLE INFO

Keywords:
Sediment connectivity
Shallow landslides
erosion mitigation
Silvopastoralism
Cost-effectiveness

ABSTRACT

In silvopastoral environments, landslide erosion results in loss of productive soils and pasture. Sediment delivered to streams from landslides contributes to the degradation of freshwater and marine receiving environments by smothering benthic habitats and increasing turbidity, light attenuation, and sediment-bound contaminants. Biological mitigation is an important strategy in pastoral environments to combat landslide erosion and improve the health of downstream aquatic ecosystems. Using lasso logistic regression, we investigate determinants of sediment connectivity for a landslide-triggering storm event in 1977 in the Wairarapa, New Zealand. Furthermore, we develop the first morphometric connectivity model to predict the likelihood of sediment delivery to streams following landslide initiation. We explore a range of connectivity scenarios by defining a set of sinks and simulating varying rates of sediment generation during flood events of increasing magnitude. The likelihood of sediment delivery is greatly enhanced where landslide deposits coalesce. Besides scar size variables, overland flow distance and vertical distance to sink were the most important morphometric predictors of connectivity. When scar size variables were removed from the connectivity model, median AUROC was reduced from 0.88 to 0.75.

By coupling landslide susceptibility and connectivity predictions in a modular form, we quantify the cost effectiveness of targeted versus non-targeted approaches to shallow landslide mitigation. Sediment delivery ratios range from 0.21 to 0.29, equating to an event sediment yield of 3548 t km^{-2} to 9033 t km^{-2}. Targeted mitigation of landslide-derived sediment is approximately an order of magnitude more cost-effective than a non-targeted approach. Compared with a pasture-only baseline, a 34% reduction in sediment delivery can be achieved by increasing slope stability through spaced tree planting on 6.5% of the pastoral land. The maximum reduction achievable through comprehensive coverage of widely spaced planting is 56%. The landslide connectivity model provides an objective method to support management decisions relating to mitigation of landslide erosion and sediment delivery to streams.

1. Introduction

Shallow landslides are an important mass wasting process and source of sediment in steep terrain and can have significant downstream impacts on freshwater and marine environments (Ziemer et al., 1991; Glade, 2003; Rahn, 2005; Broeckx et al., 2016; Dymond et al., 2017; Jia et al., 2021). In New Zealand, much pastoral farmland is predisposed to shallow landslide erosion reflecting steep and highly dissected slopes underlain by soft sedimentary rocks (Basher, 2013). Following European settlement, deforestation of a large part of the country for pastoral farming has accelerated landslide erosion rates (Glade, 2003; Fuller and Rutherfurd, 2021). Shallow translational landslides occur within the material above the bedrock, i.e., the regolith which includes soil, saprolite, colluvium and deposits of tephra and loess (Crozier, 1996; Phillips et al., 2021). They are small, shallow rapid failures that have been identified as the most common type of mass movement in the New Zealand landscape (Basher, 2013; Smith et al., 2021; Spiekermann et al., 2022). Shallow landslides have also been referred to as earth flows (e.g., Crozier, 1996) or mud flows (Geertsema et al., 2010) reflecting movement as liquified material (Cruden and Varnes, 1996). Periodic high-intensity rainfall events regularly trigger large numbers and high densities of shallow landslides (Crozier, 2018). The landslide deposits of

* Corresponding author at: Manaaki Whenua – Landcare Research, Palmerston North, New Zealand.
E-mail address: spiekermannr@landcareresearch.co.nz (R.I. Spiekermann).

https://doi.org/10.1016/j.ecoleng.2022.106676
Received 8 February 2022; Received in revised form 29 March 2022; Accepted 27 April 2022

shallow landslide scars (50–100 m^2; Betts et al., 2017) are typically long and narrow and may coalesce with adjacent landslide deposits to transport and deposit fine sediment in freshwater streams below (Mondini et al., 2011; Kasai and Yamada, 2019; Bessette-Kirton et al., 2020). In the long-term, shallow landslides can seriously degrade the soil resource (De Rose, 1993; Lambert et al., 1984) and, as an important source of sediment, contribute to the degradation of freshwater quality and marine receiving environments (Hicks et al., 2011; Davies-Colley, 2013).

The importance of shallow landslides as a contributor to catchment sediment budgets is spatially and temporally variable as a function of i) the predisposition of the terrain to landsliding, ii) the frequency and magnitude of both the triggering mechanism (e.g., rainfall) and the response (i.e., the landslides), and iii) sediment connectivity that determines off-slope sediment delivery rates. Sediment connectivity describes both the potential and proficiency of a catchment to facilitate the conveyance of sediment between its components (Heckmann and Vericat, 2018), that is, the transfer of sediment from a source to sink via sediment detachment and transport (Bracken et al., 2015; Najafi et al., 2021). There are a variety of landforms and scales where connected sediment transfer takes place. These include on hillslopes, between hillslopes and channels, and within channels (Brierley et al., 2006; Fuller and Death, 2018). Connectivity is an important concept as it can help anticipate downstream impacts of hillslope erosion. When considered as a functional, process-based framework (Bracken et al., 2015), it can help increase understanding of how erosion and sediment delivery to streams can have severe downstream effects on water quality and ecosystem health (Dymond et al., 2017). Moreover, consideration of connectivity is essential from a sediment management perspective, for example prioritizing erosion mitigation on hillslopes to reduce sediment delivery to streams or to improve sediment continuity in catchments (Simoni et al., 2017). Therefore, this study is concerned with sediment connectivity in terms of lateral linkages that drive the supply of materials from slopes to the channel network (Brierley et al., 2006).

Silvopastoralism has been widely adopted as a sustainable land management and soil conservation tool in New Zealand (Wall et al., 1997; Benavides et al., 2009; Mackay-Smith et al., 2021). A primary objective in integrating trees into pastoral hill country is the prevention of hillslope erosion and delivery of sediment to streams (Thompson and Luckman, 1993; Basher et al., 2020; Spiekermann et al., 2021, 2022), since high sediment connectivity can have detrimental outcomes on riverine and estuarine habitats by reducing the diversity, types, and abundance of fauna (Fuller and Death, 2021). The introduction of sediment standards into New Zealand's National Policy Statement for Freshwater Management (NPS-FM) has required regional authorities to manage freshwater in a way that considers the effects of land-use, including the effects on receiving estuarine environments (New Zealand Government, 2020). From a sediment mitigation perspective, both potential landslide source areas and mobilisation of sediment from source to channel need to be assessed to support targeted erosion control through tree planting. In general, targeting mitigation actions to critical source areas greatly increases the cost-effectiveness of measures (Doody et al., 2012; McDowell, 2014; McDowell et al., 2018). Cislaghi and Bischetti (2019) proposed a modular approach to couple slope stability modelling and connectivity. Similar methods have been used for modelling sediment delivery from debris flows (Burton and Bathurst, 1998), surface erosion (Poeppl et al., 2019; Zhao et al., 2020; Najafi et al., 2021b), and large wood recruitment to streams (Rigon et al., 2012; Lucía et al., 2015). These approaches adopt either physical or statistical models to predict slope stability, followed by a prediction of run-out length to determine the degree of connectivity. While landslide connectivity models have been categorised by various authors (e.g., Rickenmann, 2005; Cislaghi and Bischetti, 2019; Najafi et al., 2021), the most common methods use either a limiting criterion (e.g., involving critical slope and deposition zone; e.g., Bathurst et al. (1997) or Dymond et al. (2006)), or some variation of an empirically fitted relationship between landslide volume and runout length (e.g., Cislaghi and Bischetti, 2019), which may be extended to include additional factors influencing run-out distance such as travel angle or fall height (Corominas, 1996; Bessette-Kirton et al., 2020). Other approaches to identify erosion source and deposition areas include the use of repeat digital elevation models (Croke et al., 2013; Heckmann and Vericat, 2018; Scheipp and Wegmann, 2022), mathematical graph theory (Heckmann and Schwanghart, 2013), and a two-parameter friction model (Wichmann et al., 2009).

The index of connectivity (IC) developed by Borselli et al. (2008) and further developed by Cavalli et al. (2013) has been widely adopted. Najafi et al. (2021a) reviewed the IC and discussed its limitations, which relate to the interpretation of the index as well as the lack of quantitative validation. However, the IC has been successfully used as a predictor of muddy flood-affected sites (De Walque et al., 2017) and sediment transfer between sediment sources (e.g., landslides, debris flows, sheet, and rill erosion) and water channels (e.g., Najafi et al., 2021b; Martini et al., 2022). Najafi et al. (2021a) also made an important distinction between structural and functional connectivity concepts. The IC aims to represent structural sediment connectivity based on (high-resolution) topographic influences on sediment flux. Since the IC fails to represent process-specific characteristics of sediment source and transport, inconsistencies can arise when comparing IC values to process-specific modelling (Cislaghi and Bischetti, 2019; Poeppl et al., 2019; Zhao et al., 2020). Thus, the IC is a useful tool for representing structural connectivity but is less well suited for modelling functional connectivity (Martini et al., 2022).

Against this background, we follow a modular approach proposed by Cislaghi and Bischetti (2019) for shallow landslides by coupling a landslide susceptibility model with a connectivity model. Since the use of universal empirical relationships between scar size and run-out distance is known to perform poorly because it disregards multiple factors that determine connectivity (Corominas, 1996; Cislaghi and Bischetti, 2019), we develop the first statistical connectivity model for shallow landslides using binary logistic regression. The advantages of this approach are its limited data requirements, which consist of a high-resolution DEM for generating morphometric predictors and mapped landslide scars and deposits used to fit the model.

In addition, we consider a range of sediment delivery scenarios by defining a series of sinks and short- to long-term sediment stores in recognition of the observed variation in run-out behaviour – from insipient failures to strong, stiff plastic flows and – in their most fluid state, a slurry flow of material (Crozier, 1996). This allows a preliminary investigation of temporal dynamics in connectivity and considers the potential for deposited material to be reworked during subsequent rainfall events, for example, increased recruitment of sediment by overland flow across saturated soils adjacent to streams. A further objective of this paper is to assess sediment delivery from shallow landslides under different land management scenarios at the scale of widely spaced individual trees. We quantify sediment delivery reductions compared to a pasture-only baseline using the following conditions: 1) existing tree cover, 2) targeted mitigation to slopes with high landslide susceptibility and high sediment connectivity, and 3) complete tree cover using a 15 × 15 m grid of poplar trees. Predictions are made for 50 pastoral farms in the Wairarapa hill country to quantify the reductions in sediment delivery from shallow landslides under the different land management scenarios. We also 1) provide an assessment of cost effectiveness based on the number of trees required to achieve the respective outcomes, 2) quantify the cost-effectiveness of targeted versus non-targeted erosion control, and 3) discuss the implications for land management.

2. Data and methods

2.1. Study area

An inventory comprising shallow landslide scars and deposits mapped across a 700-ha area of steep pastoral farmland east of Masterton in the Wairarapa of New Zealand (Fig. 1) forms the basis of the present study. The study area is part of a 1700 ha sheep and beef farm, which has been the focus of many previous studies on soil erosion (e.g., Crozier et al., 1980; Lambert et al., 1984; Rosser and Ross, 2011; De Rose, 2013; Basher et al., 2018; Spiekermann et al., 2021; Spiekermann et al., 2022). The layer of indigenous vegetation was cleared for pastoral farming between 1860 and 1890 (Lambert et al., 1984). Besides small patches of naturally regenerating *Leptospermum scoparium* (mānuka) and *Kunzea* spp. (kānuka) visible in historic imagery, woody vegetation was largely absent in the study area until the 1980s when soil conservation works began to populate hillslopes with widely spaced poplar, willow, and eucalyptus trees. The morphology is best characterised by its steep, highly dissected terrain with narrow ridge and spur crests, hillslopes mostly between 15° and 35° that are underlain by highly erodible Neogene-aged sedimentary rocks. These consist mostly of massive, poorly bedded sandstone and coarse siltstone, partially overlain by a loess mantle. Brown loamy soils (Waitataura_14a.1) are most common in the study area and are moderately well drained (Lilburne et al., 2012). However, a dense subsoil zone of slow permeability provides a failure plane for shallow landslides (De Rose, 2013). Gley soils (Taihape_10a.1; Lilburne et al., 2012) are commonly found on the lower slopes and valley bottoms. A large gully has formed in the northern section of the study area within an area of massive mudstone. To the west of the gully, an area largely devoid of landslides is part of a band of coquina limestone that extends farther to the south-west of the study area. Mean annual rainfall is approximately 1100 mm, with wet winters and dryer summers the norm.

2.2. Data and data preparation

2.2.1. Landslide inventory

Beginning 18/09/1977, a rainfall event lasting five days (with 137 mm rainfall recorded at the nearest weather station – Gladstone) caused very extensive shallow landsliding in the Wairarapa hills (De Rose, 2013). Wet winter months preceding the rainfall event contributed to high antecedent soil moisture conditions. An aerial survey captured photography at a scale of 1:25000 shortly after the event, on 10/10/1977, which allowed scars and landslide deposits to be identified and differentiated (Fig. 1). Mapping was enhanced by producing raster objects via the multiresolution segmentation algorithm in eCognition using the panchromatic image from 1977, the DEM and slope grids as inputs. Scars and landslide deposits were classified based on the brightness (mean and standard deviation) of image objects and a slope gradient threshold of 30° aimed at removing most false positives. Image objects adjacent and at lower elevation to mapped scars were classified as landslide deposits while increasing thresholds for mean slope and brightness to allow for greater variation caused by conglomerates of turf and sediment in image objects. The process of landslide deposit classification was done iteratively to allow landslide deposits to expand downslope. Manual refinement of the classification was performed across the entire study area by selecting and removing falsely classified objects. The ruleset description can be viewed in the supplementary material. The final landslide inventory includes 2002 scars and 1216 landslide deposits. Of these scars, 446 have no obvious landslide deposit, which suggests these may represent incipient failures or intact rafts of turf. A further 571 scars had a single deposit, whereas the remaining 985

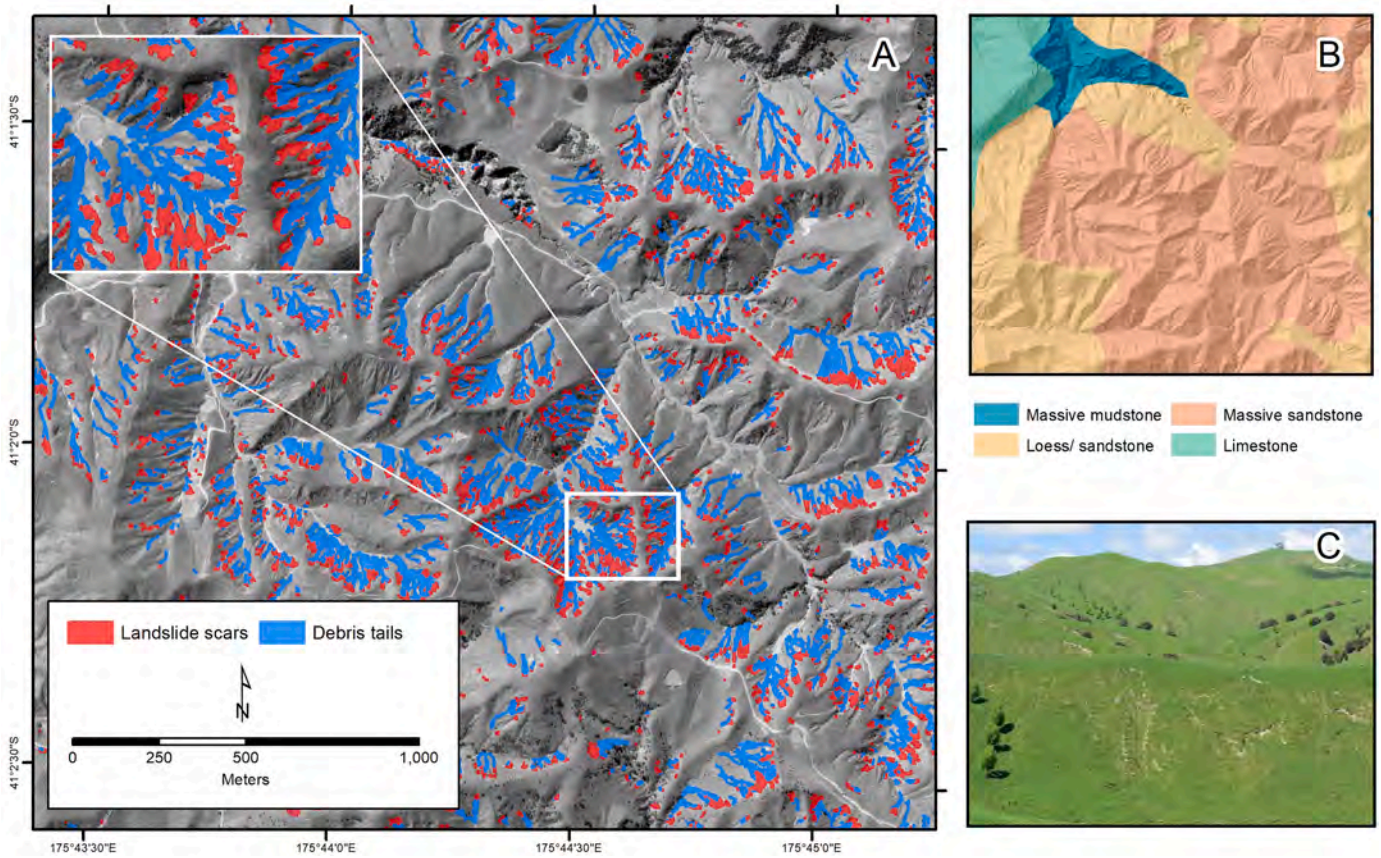

Fig. 1. Insert A: 1977 imagery with landslide scars and deposits; Insert B: Lithology; Insert C: Landscape photo within study area showing steep, deeply dissected terrain (Source: Ebony Davison). Note: Location of study area in New Zealand is shown in Fig. 3.

scars have landslide deposits that coalesced with adjacent landslide deposits.

2.2.2. Landslide connectivity scenarios

In this study, landslide connectivity is operationalized through a simple definition: A shallow landslide is defined as connected when its landslide deposit intersects with a pre-defined sink, which we refer to as a connectivity target. This definition results in a binary classification of landslide scars as "connected" (LC) or "unconnected" (LU), and therefore lends itself to a statistical investigation of the factors that determine connectivity based on a Bernoulli distribution. In addition, this study aims to investigate the dependence of connectivity on the definition of the connectivity target by assessing changes to the Bernoulli distribution as well as change in effect size of variables. Therefore, we define a set of six connectivity targets using a LiDAR-derived stream network and the topographic wetness index (TWI). The varying connectivity targets are designed to test the effect of different catchment hydrological conditions on sediment delivery. This allows exploration of how timing of landslides either within-storm or differences in soil wetness between storms may affect sediment delivery.

The first connectivity target is defined by a stream network that was generated using the 1-m DEM, following the standard procedure of filling terrain depressions with the Fill Sinks XXL function (proposed for LiDAR DEM processing by Wang and Liu, 2006) and a flow algorithm (Quinn et al., 1991). A stream initiation value of 6400 m^2 was set, which was identified as a suitable threshold in mudstone terrain for permanent, intermittent, and ephemeral streams (Storey and Wadhwa, 2009). The streams were buffered by 5 m and the polygon used to represent the first of six targets. We refer to this connectivity target as "Streams".

The remaining five connectivity targets were defined using the TWI, which is a measure for accumulated water or soil saturation (Moore et al., 1988; 1991), calculated as:

$$TWI = ln\left(\frac{SCA}{sg}\right)$$

where *SCA* is the specific catchment area, and *sg* is slope gradient in radians. We set the minimum slope in the filled DEM to 0.01 rad to avoid division by zero during TWI calculation (Kopecký et al., 2021). Slope was calculated using the 3rd degree polynomial with 10 parameters (Haralick, 1983), which is the slope algorithm that performed best when used to predict measured soil moisture as a component of TWI (Kopecký et al., 2021). Targets were then defined using TWI thresholds based on the distribution of TWI values in the study area (Fig. 1b). The thresholds used to represent potential zones of saturated soils correspond to the 75, 80, 85, 90, and 95th percentiles of the TWI distribution in the study area. A lower cut-off corresponds to a larger hypothesized zone of saturated soils, which has the effect of increasing the ratio of scar connectivity (Fig. 2c; Table 2). TWI zones unconnected from the stream network were removed. Therefore, the TWI-based connectivity targets are upslope extensions to the stream network. While the transport capacity of sediment in these TWI zones is unknown, we expect sediment delivery to decrease with increasing size of the TWI connectivity target, as there are more opportunities for deposition to occur on footslopes and floodplains during the overland flow phase between landslide deposition and subsequent erosion/transport through the TWI-defined saturated area to the stream channel. Thus, while an increasing proportion of landslide deposits intersect the larger connectivity targets, the average proportion of source material that is ultimately delivered into the stream channel is reduced compared to landslide deposits delivering directly to the stream channel.

We differentiate these two aspects of sediment delivery by quantifying the landslide connectivity ratios (the proportion of landslides

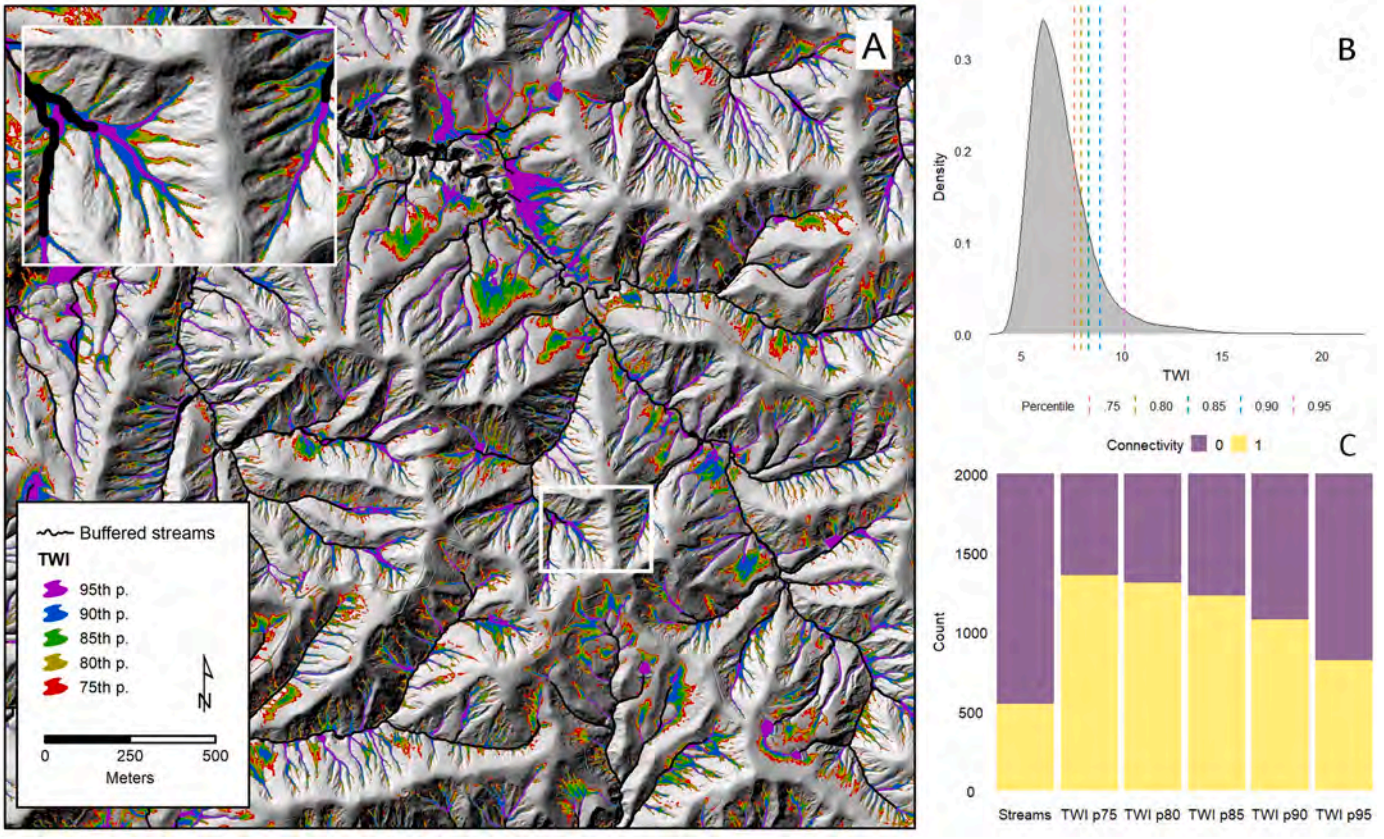

Fig. 2. Insert A: Stream network and TWI-based sinks set using percentiles from the distribution shown in Insert B; Insert C: Number of landslide scars connected (1) and unconnected (0) based on intersection of landslide deposits with respective sinks.

connecting to target) and sediment delivery ratios (SDR) for each respective target. The SDRs were based on the scar area/volume of connecting landslides. For the *Streams* target, we assumed that, on average, connected landslides delivered 50% of mobilised sediment to sink (Reid and Page, 2002; Jones and Preston, 2012). For sediment deposited to the *Streams* target, sediment transport in the channel network is accelerated by in-stream processes.

We consider SDR to be both a function of 1) the LCR (number of landslide deposits connecting to target) and 2) the capacity to maintain sediment transport from source (landslide scar) to sink (stream). Therefore, we assume the rate of delivery to the water channel is reduced by increments of 5% with each successive TWI-based connectivity target (TWI-p.95: 45% – TWI-p.75: 25%) to reflect the hypothesized reduction in transport capacity from the initial landslide deposition and subsequent transport of sediment to stream channel by overland flow – either within or post rainfall event. In the absence of empirical evidence to support this assumption, this approach is aimed at modelling the reduction in recruitment and transport capacity in areas of increasing distance from the water channel to explore the dependence on assumptions related to sink definition and transport capacity. Besides distance, the roughness in surface morphology of footslopes and toeslopes may impede particles being entrained in overland flow. SDRs thus describe the proportion of all mobilised material entering the watercourse or to an area where overland flow is likely to allow sediment transport to continue, albeit at a reduced rate. The TWI-based connectivity targets are, thus, designed to characterize potential increases in SDR through surface run-off erosion post rainfall event (Xiong et al., 2022). In addition, we compute sediment yields for the landslide triggering event, assuming soil bulk density is 1.4 t m^{-3} and an average scar depth of 1 m (Crozier, 1996).

2.2.3. Explanatory variables

The most common approach for estimating sediment delivery from landslides to streams is to develop empirical relationships between soil volume and run-out distance, which may be further refined by considering the vertical drop (Rickenmann, 1999). Therefore, an important explanatory variable that determines runout-distance is the initial soil-involved landslide volume (Corominas, 1996; Crozier, 1996; Cislaghi and Bischetti, 2019). We include landslide scar area (ScarArea) as an explanatory variable in the models. Scar area is a reasonable substitute for volume, since shallow landslides tend to have small depth to area ratios (Betts et al., 2017). To test the influence of multi-source landslide deposits on the mobility of sediment material, we also include the total area of all scars (SumScAr) contributing to any given landslide deposit as a second variable related to the volume of source material.

The LiDAR digital terrain model (DTM) from Greater Wellington Regional Council was used at 1-m resolution to generate a set of fourteen morphometric explanatory variables to investigate their importance as predictors of connectivity (Table 1). Because landslides were triggered in 1977 prior to the LiDAR survey, a median filter with 3-m radius was used to remove minor surface roughness produced by the shallow landslide scars (ca. 1 m depth; Betts et al., 2017) to approximate the terrain surface prior to failure. Each landslide scar was converted to a centroid point (forced inside polygon) and morphometric variables were extracted at the location of points. The variables were standardized (centred around the mean and scaled by the standard deviation) prior to fitting models to allow comparison of coefficient estimates.

Flow Accumulation is the accumulated count of cells flowing into any given cell (m^2). Flow accumulation is therefore a measure for topographic location with respect to catchment and a proxy for (potential) surface runoff. Due to the high positive skewness, a log-transformation of flow accumulation was used. *Distance to Channel* is the overland flow distance (m), whereas the *Vertical Distance to Channel* is the altitude difference (m) to a pre-defined channel network (see Section 2.2.2). *Slope Height* (standardized) and *Valley Depth* are relative measures for slope position (Böhner and Selige, 2006). *Valley Depth* is the normalized difference between slope height and valley depth. *Easternness* uses the sine transformation of slope aspect (*dx*); *Northernness* the cosine transformation (*dy*) since aspect is a circular variable. *Slope gradient* is the gradient at the centroid of the scar (°; Zevenbergen and Thorne, 1987); Crozier (1996) found a significant correlation ($P < 0.05$) between the surface angle of rupture and runout distance. We include the *Downslope Distance Gradient* (Hjerdt et al., 2004), $\tan\alpha_d = d/L_d$, where L_d is the horizontal distance to the point with an elevation d meters below the elevation of the starting cell, following the steepest-direction flow path. The gradient aims to quantify topographic controls on local hydrology – specifically groundwater table gradients that are less dependent on local surface slope. We hypothesize that the *Downslope Distance Gradient* is important for sediment delivery as it captures landform-scaled slope gradient in contrast to local surface slope. In consideration of raster resolution (1 m) and topography, we selected a *d*-value of 50 m. *Gradient Difference* is the unitless difference between $\tan\alpha_d$ and local surface gradient (Hjerdt et al., 2004). The *Topographic Positioning Index* compares the elevation of each cell in a DTM to the mean elevation of a specified neighbourhood around that cell (Guisan et al., 1999). Thus, high values correspond with local high points such as ridges, low values

Table 1
Morphometric explanatory variables used in connectivity model. All variables are continuous and calculated at 1-m resolution.

	Morphometric explanatory variable	Algorithm	Parameterization
1	Log-transformed flow accumulation (LogFA)	Package: RSAGA, Library: ta_channels, Module: 0	Method: Multiple Flow Direction (MFD) Convergence = 1
2	Distance to channel (DisOvrlnd)	Package: RSAGA, Library: ta_channels, Module: 4	Method: MFD
3	Vertical distance to channel (VDis)	Package: RSAGA, Library = ta_channels, Module = 4	
4	Slope Height (SlopeSH)	Package: RSAGA, Library = ta_morphometry, Module = 14	w = 0.5, t = 15, e = 2
5	Valley depth (SlopeVD)	Package: RSAGA, Library = ta_morphometry, Module = 14	w = 0.5, *t* = 15, e = 2
6	Easternness	Package: qgisprocess: grass7:r.slope.aspect	
7	Northernness	Package: qgisprocess, grass7:r.slope.aspect	
8	Slope gradient (Slope)	Package: RSAGA, Library: ta_morphometry, Module: 0	
9	Downslope distance gradient (Gradient)	Package: RSAGA, Library: ta_morphometry, Module: 9	d = 50
10	Gradient difference (GradientDif)	Package: RSAGA, Library: ta_morphometry, Module: 9	d = 50
11	Topographic Position Index (TPI)	Package: RSAGA, Library: ta_morphometry, Module: 18	r_min = 3, r_max = 30
12	Topographic Wetness Index (TWI)	Package: RSAGA, Library: ta_hydrology, Module: 20	
13	Topographic ruggedness index (TRI)	Package: RSAGA, Library: ta_morphometry, Module: 16	r = 10
14	Vector Ruggedness Measure (VRM)	Package: RSAGA, Library: ta_hydrology, Module: 17	r = 4

with local low points such as valley bottoms. The *Topographic Wetness Index* is a measure of water accumulation or soil saturation (Moore et al., 1988), which may influence sediment viscosity of the mobilised material, and also the propensity for surface runoff generation. The *Topographic Ruggedness Index* is a measure of topographic heterogeneity within a defined radius ($r = 10$ m; Riley et al., 1999) and is hypothesized to influence the downslope depositional rate (Crozier, 1996). Similarly, the *Vector Ruggedness Measure* decomposes slope and aspect into 3-dimensional vectors and calculates the resultant vector magnitude within a user-specified moving rectangular window ($r = 4$ m; Sappington et al., 2007). Each of these variables was processed in R (R Core Team, 2021) using the packages RSAGA (v. 1.3.0; Brenning et al., 2018) or qgisprocess (v.0.0.0.9; Dunnington, 2021) and extracted to points using the raster package (v.3.4–13; Hijmans, 2021).

2.3. The landslide connectivity model

2.3.1. Binary logistic regression with LASSO

The statistical evaluation of landslide connectivity aims to test the importance of the selected morphometric variables in determining sediment delivery from hillslopes to streams. For each of the six connectivity targets (Section 2.2.2), an equal number of connected and unconnected landslide points were selected. Depending on the connectivity target, the number of connected landslides differ between the minimum of 546 connected to the Streams target and a maximum of 1388 for the TWI-75 target (Table 2). As the area of the zone defined as the target increases, the degree of landslide connectivity increases. Therefore, where the ratio of Landslide-Connected to Landslide-Unconnected (LC:LU) <1, we selected all connected landslide points and an equal number of randomly sampled unconnected landslide points, and vice versa where the ratio LC:LU >1. These balanced sets of landslide points constitute the binary response variable (LU = 0, LC = 1) with the corresponding independent explanatory variables (Table 1).

We developed the connectivity models using logistic regression, which models the probability of a binary response variable ($Y = 0|1$) with a Bernoulli distribution. Logistic regression uses the maximum likelihood estimator to determine parameters β_0 and β_1 to find optimum probability values given a set of predictor variables x_i. Variable selection was automated with the *Least Absolute Shrinkage Selection Operator* (lasso; Tibshirani, 1996). The advantage of the lasso method is that variable selection and coefficient estimation is performed simultaneously to generate a model that optimizes for performance while avoiding over-fitting. This is achieved by minimizing the negative log-likelihood function (Hastie et al., 2009; Akalin et al., 2020):

$$-ln(L) = -\sum_{i=1}^{n}\left[-ln\left(1+e^{(\beta_0+\beta_1 x_1+\ldots\beta_i x_i)}+y_i(\beta_0+\beta_1 x_1+\ldots\beta_i x_i)\right)\right]$$

by adding a penalty term that forces coefficients to be shrunk towards 0, where p is the number of variables in the model:

$$-ln(L)+\lambda\sum_{j=1}^{p}|\beta_j|$$

The penalty term is determined by the parameter λ which controls the sparsity of the estimator, i.e., the number of coefficients shrunk to 0. The optimal tuning parameter is found by testing a range of values in a cross-validation to reduce out-of-sample error. Lasso regression was implemented in R using the caret (Kuhn, 2020) and glmnet (Friedman et al., 2010) packages. The raster package was used for model predictions (Hijmans, 2021).

2.3.2. Sampling design and model evaluation

To test the consistency of variable selection, estimation of coefficients, and model performance across the six connectivity targets, we repeatedly sampled from the landslide dataset to generate 100 balanced datasets, whereby $n = \min\{LC, LU\}$ (Table 2). This process is repeated for each of the six connectivity scenarios resulting in 600 models. Each model was tuned to determine the optimal λ value (range 0.001–0.1 by 0.001 increments) using k-fold cross validation ($k = 10$). Samples were randomly partitioned into k folds, whereby $k - 1$ folds were used to train the model and the remaining fold used to test the predictive ability of the model. This was repeated until each of the ten folds was used for model testing.

Since logistic regression results in predicted probabilities of class association, a probability cut-off needs to be selected for binary classification and model validation. The selection of cut-off can be varied depending on the purpose of the model which may influence the tolerance of certain true positive or false positive rates. For this reason, the area under receiver operator curves (AUROC) is commonly used to estimate model performance as it is a threshold-independent performance measure (Brenning, 2005). Receiver operator curves plot the true positive rate (sensitivity) against false positive rate (1 – specificity) across all potential cut-offs (0–1). The AUROC is therefore a suitable measure to summarize a model's prediction performance for balanced samples as it does not depend on the cut-off used to calculate classification accuracy (Hosmer and Lemeshow, 2000). An AUROC score of 1 would mean the model can perfectly discriminate between connected and unconnected landslides in its predictions; a value of 0.5 corresponds to no discriminatory power and is equal to that achieved by pure chance. A good AUROC score is considered to lie between 0.8 and 0.9; an excellent score > 0.9 (Safari et al., 2016; El Khouli et al., 2009).

Variable importance is assessed using inclusion rate and the size of standardized coefficient estimate values. Based on results of k-fold cross-validation, the model with the highest median AUROC was selected from the 100 repetitions for each of the six targets and used to quantify model fit and prediction skill. Model fit was estimated by quantifying AUROC and maximum accuracy using predictions on the entire unbalanced dataset of 2002 landslide scars. Maximum accuracy uses the probability threshold (= cut-off) that renders a binary classification with the highest accuracy. Given that the datasets are unbalanced across all six targets (Table 2), the optimal cut-off can deviate from 0.5. The predictive skill was quantified through AUROC for each of the ten folds using cross-validation and evaluated using boxplots.

Generating accurate predictions of landslide size is an active research field – both in the domain of physical-process-based modelling (e.g., Bellugi et al., 2015a, 2015b) and statistical modelling (Lombardo et al., 2021). Moreover, coalescing landslides were hypothesized to be an important determinant of landslide connectivity and were therefore investigated by inclusion of the total area of all scars contributing to a

Table 2
Number and scar size (mean, standard deviation) of connected and unconnected landslide scars, as well as fraction ground eroded by connected and unconnected landslide scars.

	Streams	TWI-p.75	TWI-p.80	TWI-p.85	TWI-p.90	TWI-p.95
Landslide scars - connected (LC)	546	1388	1311	1227	1078	809
Landslide scars - unconnected (LU)	1456	614	691	775	924	1193
Mean (SD) scar size – LC (m^2)	156 (229)	127 (176)	129 (180)	133 (184)	137 (192)	145 (204)
Mean (SD) scar size – LU (m^2)	82 (105)	47 (401)	52 (52)	55 (56)	62 (68)	74 (96)
Fraction ground eroded - LC (%)	0.122	0.252	0.242	0.232	0.211	0.122
Fraction ground eroded - LU (%)	0.171	0.041	0.052	0.061	0.082	0.171

given landslide deposit (SumScAr). However, given the challenges associated with forecasting landslide size, location, and density, we investigate how well morphometric variables can predict connectivity without knowledge of the size of mobilised source material. The scar size variables are thus removed to both test the sensitivity of the models to the size of mobilised source material and investigate the extent to which morphometric variables can predict connectivity without prior knowledge of scar size or density. We refer to the two model runs as "scar-size models" and "morphometric models". Spatial predictions of connectivity (Section 2.4) for the land management scenarios are based on the morphometric model which includes only topographic effects.

2.4. Land management scenario modelling

2.4.1. Landslide susceptibility

We followed a modular approach to couple potential source areas through landslide susceptibility and sediment delivery through connectivity models (Cislaghi and Bischetti, 2019). We use the landslide susceptibility model developed by Spiekermann et al. (2022), which is based on a landslide inventory of approximately 43,000 scars that were triggered between 2005 and 2009. Landslide scars were mapped in the Wairarapa pastoral hill country overlapping the study area (Fig. 3). Predictor variables include slope gradient, aspect, lithology, and tree influence models on slope stability (TIMSS) that represent the influence of individual trees for four different vegetation types). TIMSS were

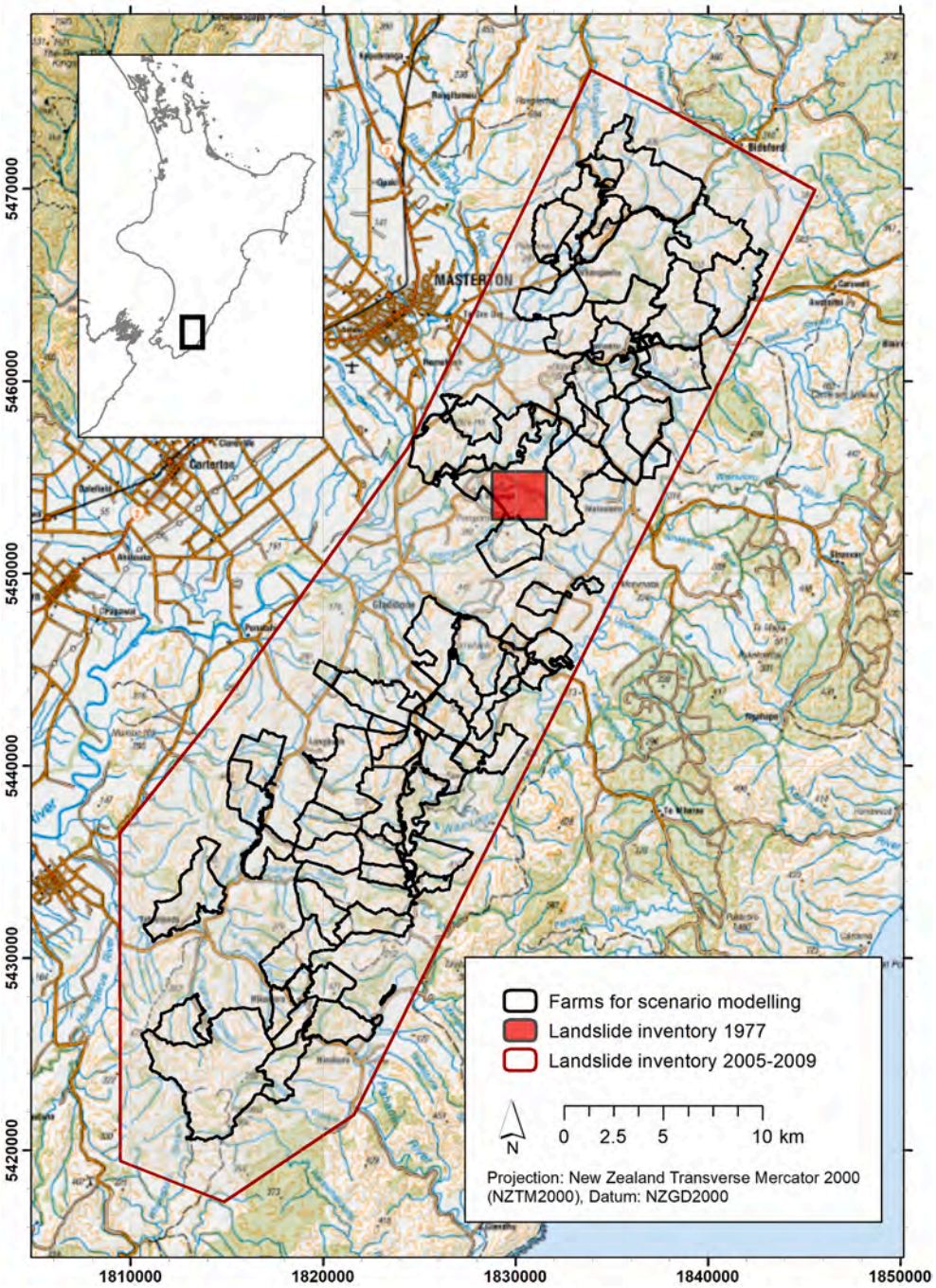

Fig. 3. Location of study area of the 1977 landslide inventory used for the connectivity model, the extended study area of the 2005–09 landslide inventory used by the landslide susceptibility model, and the location of 50 farms selected for the land management scenarios.

developed for different tree types based on an empirical relationship between distance from tree and reduction in soil surface eroded. The models are spatial representations of this relationship (1-m pixel), following a sigmoidal shape until reaching an asymptotic value denoting the distance at which the tree has no observable influence on slope stability (Spiekermann et al., 2021, 2022). TIMSS are normalized to 0–1 but can exceed values of 1 due to the additive contributions from multiple trees. TIMSS are produced for the dominant tree types in the study area, which include eucalyptus, kānuka, poplar/willow and coniferous tree species. Binary logistic regression was used to develop the susceptibility model and model performance using k-fold cross-validation was excellent (AUROC of 0.95).

2.4.2. Coupling landslide connectivity and susceptibility

We integrated predictions of landslide connectivity and susceptibility using a modular approach. First, spatial predictions were reclassified into three classes, "Low", "Medium", and "High". Class thresholds were determined by ranking landslide scars in decreasing order by their probability values. The probability values associated with the 5th and 15th percentiles were then selected. For the landslide susceptibility classification (Spiekermann et al., 2022), these values correspond to 0.32 and 0.72, which means that 80% of landslide scar points had probability values >0.72, 15% had values between 0.32 and 0.72 and the remaining 5% had probability values <0.32 (Spiekermann et al., 2022).

The same procedure was used for the predicted probabilities of landslide connectivity using the connected landslide scars and ranking these in descending order by their probability values. Similarly, the high connectivity class can be interpreted as being the zone where 80% of connected landslides were triggered, which we refer to as the connectivity rate. An intersection of the two reclassified spatial predictions resulted in a matrix of nine classes describing both the likelihood of landsliding to occur in future and the potential for sediment to be delivered to the respective target.

Landslide connectivity ratios (LCR) were computed for each of the connectivity classes (i = 3) for the six morphometric models based on the number of landslides connecting (LC_j) to each jth target (j = 6) of the total number of landslides in the inventory (L_N). The class-specific connectivity rate (CR_i) is 0.8 for the high connectivity class, 0.15 for medium, and 0.05 for the low class:

$$LCR_{ij} = \frac{LC_j}{L_N} \times CR_i$$

SDRs were calculated for each connectivity class i in a similar way based on the volume of connected scars (LCV_j) relative to total landslide scar volume (L_V), for the class-specific proportion of the connected scar volume (that differs with target j) (CP_{ij}). For example, for j = Streams, 0.77 of the volume of material from connected scars (LCV_j) was sourced from the high class, 0.19 from the medium class and 0.04 from the low class. The target-specific delivery rate (DR_j: 0.5 for Streams, 0.45 for TWI-95, etc.; Section 2.2.2) must also be considered, as follows:

$$SDR_{ij} = \frac{LCV_j}{L_V} \times CP_{ij} \times DR_j$$

These SDRs are used to calculate class-specific event sediment yields (ESY_{ij}; t/km^2/yr) for each of the jth targets (j = 6) as follows:

$$ESY_{ij} = \frac{SDR_{ij} \times LCV_j}{A_{ij}} \times \rho$$

As mentioned in Section 2.2.2, we here assume soil bulk density ρ is 1.4 t m^{-3}. A_{ij} refers to the area occupied by class i using modelled predictions of landslide connectivity based on the jth target. The total event sediment yield is the sum of the delivered class-specific loads across the study area divided by the total mapped aera A=7 km^2.

2.4.3. Land management scenarios

To quantify the reduction in sediment delivery from shallow landslides compared to a pasture-only baseline (S_0), we developed land management scenarios to estimate the expected reductions under the following conditions: 1) actual woody vegetation as at 2013 (*WV*), 2) targeted mitigation to slopes with high landslide susceptibility and high potential for sediment delivery (S_1), and 3) complete tree cover using a 15 × 15 m grid of poplar trees (S_2). Under these scenarios, the layout and/or density of trees changes, which directly impacts on the likelihood of landslide occurrence, whereas predictions of connectivity are static due to the dependence on morphometric determinants only. The baseline is represented by a pasture-only scenario, which is achieved by setting the TIMSS variables to 0 in the landslide susceptibility model. This baseline scenario thus corresponds to the landslide susceptibility in 1977 – a landscape exhibiting a very sparse woody vegetation cover (see study area description in Section 2.1). Scenarios 1 and 2 are constructed using the poplar/willow TIMSS based on a regular grid of points representing tree locations at 15 m spacings. Values of the TIMSS model are applied as a function of distance (1-m radial increments), ranging from 1 at the tree location to 0.06 at a radius of 20 m from the simulated tree (Spiekermann et al., 2021). The resulting raster grid at 1-m spatial resolution accounts for the additive effect of the nearest four trees at any given point. Scenario 1 applies this grid across the entire farm, whereas for Scenario 2 the grid is only applied to slopes classified as both highly susceptible and with high landslide connectivity, which we refer to as targeted mitigation zones.

Predictions are made for 50 farms (>300 ha) in the Wairarapa hill country (Fig. 3) to quantify the reductions in sediment delivery from shallow landslides under the three scenarios using the buffered stream network (*Streams*) as connectivity target. Reductions in landslide erosion and sediment delivery are based on changes to the distribution of landslide susceptibility classes (CC, %) for each farm *f*:

$$CC_f = \frac{(S_x - S_0)}{S_0} * 100$$

where S_x are the proportions of the nine susceptibility/connectivity classes of scenarios S_1 and S_2, and S_0 the baseline. We assume that future landsliding will follow the same pattern as in the past, such that the majority (80%) of landslides will occur in the *high* susceptibility zone, and so forth. Therefore, a reduction in the area occupied by the *high* susceptibility zone equates to a reduction in future landslide erosion and sediment delivery. The reduction in sediment delivery (SD_{red}) considers the rate (based on counts) of landsliding LR_i and connectivity CR_i in each of the classes $i = \{0.8, 0.15, 0.05\}$:

$$SD_{red} = CC_{\%} \times LR_i \times CR_i$$

Based on the size of the farm, and the mitigation zones associated with S_1 and S_2, we calculate the number of poplar trees required to effect the modelled change. We use an average cost of $33 per plant, which is an estimate from the Greater Wellington Regional Council based on 3-m planting material, 1.7-m Dynex protection sleeve, labour and helicopter delivery (D. Boone, personal communication, November 2, 2021). We quantify the cost-effectiveness of targeted erosion control and discuss the implications for land management.

3. Results

3.1. Landslide connectivity models with scar size variables

The variable inclusion rate (%; Fig. 4a) and coefficient estimates (median; Fig. 4b) from the lasso regression model for each of the six targets suggest that the scar size variables (*ScarArea*, *SumScAr*), which represent the volume of mobilised source material, are the most important factors that determine landslide connectivity. These variables were selected in 591 of the 600 models and the effect sizes were also the

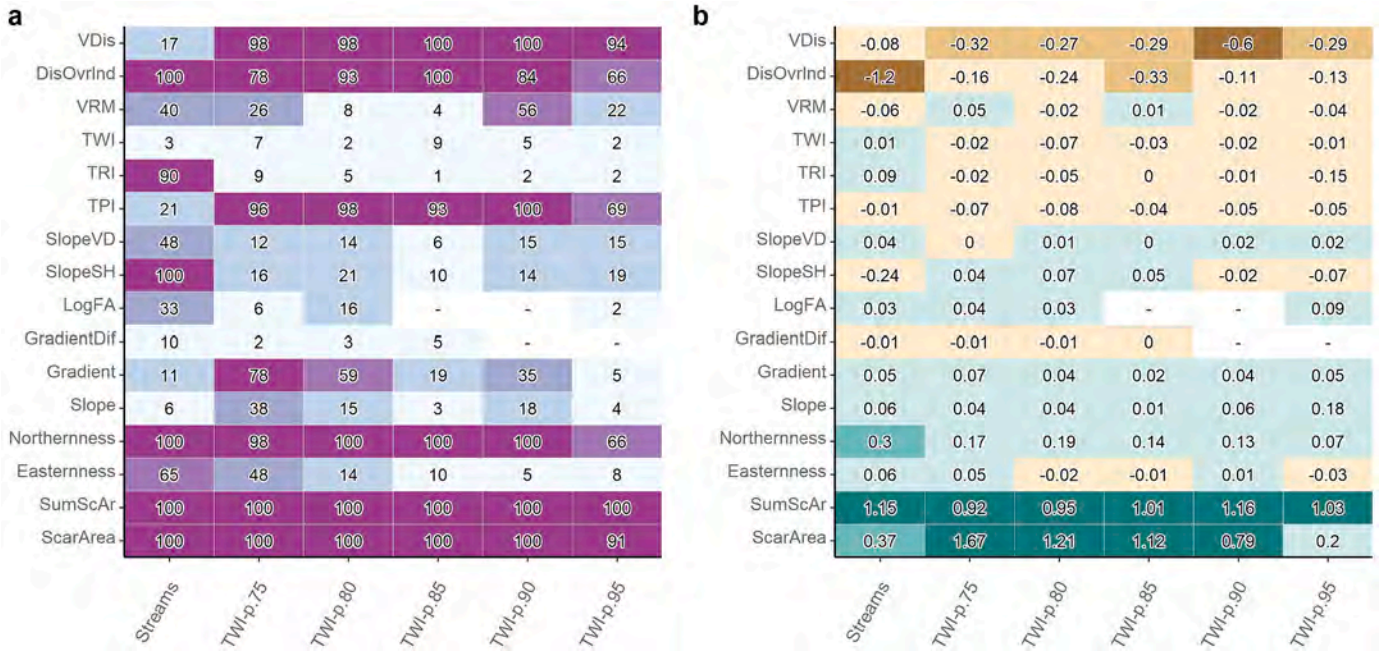

Fig. 4. Insert a): Heat-map displaying the inclusion rate of variables for all 6 connectivity targets including the scar size variables. The numbers indicate how often variables were selected for the models out of 100 estimates. Note that the sum of scar area is the only variable included consistently across all connectivity targets. Darker colours show variables selected more frequently. Grey boxes with a dash indicate which variables were never selected for the models. Insert b): Heat-map displaying estimates of coefficients (median of non-zero estimates) for all six connectivity-targets. Grey boxes are equivalent to coefficients of zero and were never selected for the models.

greatest. The results presented here further show that besides the size of individual landslide scars (*ScarArea)*, the coalescing of multiple landslides (*SumScAr*) in highly dissected hilly terrain is also an important determinant of sediment connectivity (Fig. 4). There is a notable difference in the coefficient estimates of scar size variables with respect to connectivity target. For *Streams*, *TWI-p.95* and *TWI-p.90*, which represent the targets at greater distance from slopes, the individual scar size (m^2) was not as important a factor in determining connectivity as the sum of all scars (m^2) contributing to a coalescing landslide deposit; and vice versa for the remaining three connectivity targets. This indicates that when multiple scars contribute mobilised sediment to a common landslide deposit, transportation and delivery of sediment is enhanced and can be deposited at greater distance from source. While there is an overall significant difference between individual scar sizes of connected and unconnected landslides, the difference is accentuated for *TWI-p.80 – TWI-p.75* (Table 2). Where *Streams* are set as the connectivity target, the average *SumScAr* (m^2) is almost three times greater for connected landslides (952 m^2) compared to unconnected landslides (330 m^2). On average, 6.3 individual scars contribute material to a coalescing landslide deposit compared with 2.2 for unconnected. This indicates that accounting only for the individual landslide scar size can result in underestimation of the runout distance given that landslide derived material from multiple sources can contribute to the transport of debris downslope.

Besides landslide scar size, distance is an important determinant of connectivity. Both *DisOvrlnd* and *VDis* had high inclusion rates and coefficient estimates – most notably for the *Streams* target, where *DisOvlrnd* was more important than *VDis* with a median coefficient of −1.31. Here, connectivity was found to be greater on north-facing slopes. Also noteworthy is the inverse relationship to *SlopeSH*, which may indicate higher connectivity of landslides occurring at mid-slope – where greater proximity to the stream network was more important than vertical drop. Other morphometric variables, such as *TWI*, *Slope*, *GradientDif*, *TWI* and *TRI*, were frequently shrunk to 0 and rarely included for the five TWI-based targets. Furthermore, while other morphometric variables had higher inclusion rates (*TPI*, *Gradient*), they were less important given their low median coefficient estimates. The full distribution of coefficient estimates across the 100 models as well as the estimates of the best performing model are shown in Fig. A1 (Supplementary material).

Model performance of the 100 repetitions using 10-fold cross-validations was very good for the scar-size models, and generally decreased with increasing size of the connectivity target, from a median AUROC of 0.87 for *Streams* to 0.81 for *TWI-p.75* (Fig. 5a). This means the models were best at classifying landslides as connected or unconnected when the 5 m buffered stream network was set as the connectivity target. It may reflect the importance of the combined scar size (*SumScAr*) in determining connectivity to streams and the lack of connectivity of individual scars. While only 150 of 571 landslides (26%) with 1:1 scar-desposit ratio connected, 396 of 985 (40%) with converging landslide deposits connected to target.

Model performance was further evaluated for the best of the 100 models considering both model fit and predictive skill. Model fit was excellent across all six scar-size models, with AUROCs ranging between 0.81 and 0.88, which corresponds to a maximum accuracy of 81.6% (Streams) and 75.7% (*TWI-p.80*; Fig. 6). Predictive skill is shown in the boxplots in Fig. 6. While AUROC scores are generally high, a small number of train-test iterations resulted in low AUROC scores causing large variation in predictive skill. *TWI-p.80*, *TWI-p.90* and *TWI-p.95* show the greatest variation in AUC, which points to greater uncertainty with these models. Yet in all but 4 of the 60 train-test iterations, cross-validation results across all six scar-size connectivity models had scores >0.75, which suggests these models can predict sediment delivery with a fair degree of certainty (Safari et al., 2016).

Variation in coefficient estimates is another indication for robustness in model fit, which was greatest for the scar size variables, as well as DisOvrlnd and VDis (Fig. A2) However, these are the variables with the highest inclusion rate, which likely impacts on the variability of coefficient estimates. Along with the scar size variables, these two distance variables were the most important in terms of effect size. TPI had both a high inclusion rate in the TWI-based models and low variability in the estimates of effect size. The red dots in Figs. A2 and A3 signify the coefficient values used in the best-ranked models used for spatial

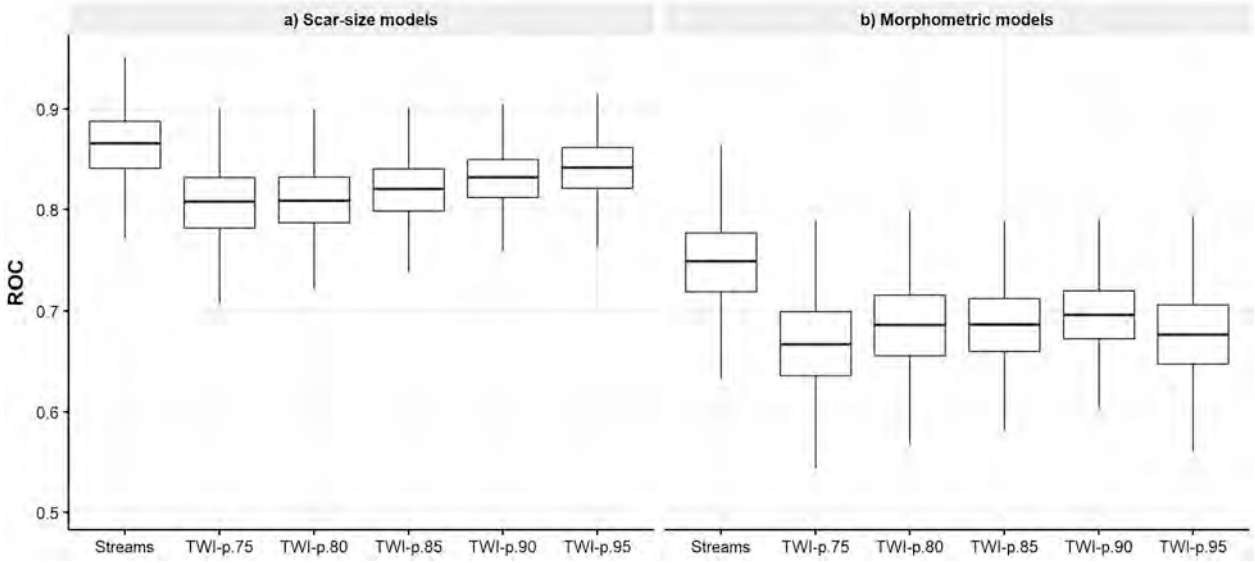

Fig. 5. Model performance (AUROC) by a) scar-size connectivity models and b) morphometric connectivity models for each of the targets. Boxplots include 100 model repetitions, each with 10-fold cross-validation. Specifically, the box indicates the interquartile range (IQR) around the median value, whiskers indicate the minimum and maximum values.

predictions.

3.2. Morphometric landslide connectivity models

The morphometric landslide connectivity models isolate the role of local topography in determining sediment connectivity. The result of removing the two scar size variables (*ScarArea*, *SumScAr*) promotes the importance of all fourteen morphometric variables included in the models. The inclusion rate is overall high, with *Northernness*, *TPI*, *Gradient*, *VDis*, *DisOvrlnd*, and *VRM* most often selected across all six targets (Fig. 7a). *TWI*, *Slope*, *GradientDif*, and *LogFA* were included less often and when included had small coefficient estimates. In terms of effect size, *VDis*, *DisOvrlnd*, *Northernness* and *Gradient* were the most important variables in determining connectivity (Fig. 7b).

However, the removal of scar size variables comes at a cost in terms of model performance (Fig. 5b), which is to be expected given the importance of these variables in the scar-size models. Across the 100 repetitions, the *Streams* connectivity model performed best, with a median AUROC of 0.75. The TWI-based models performed less well, with median AUROC ranging between 0.67 and 0.69. Of the 100 repetitions, the best-performing *Streams* connectivity model had a model fit with an AUROC of 0.76 and accuracy of 75.7% (Fig. 8). Of the six models, the *TWI-p.75* connectivity model reveals the worst model fit with an AUROC of 0.67. The remaining four TWI connectivity models have an AUROC of approximately 0.70. In terms of predictive skill, the *Streams* connectivity model outperforms the five TWI models with a median AUROC of 0.77 from 10-fold cross-validation. The range in AUROC from 0.67 to 0.84 suggests potential for both good and poor predictions. Of the TWI connectivity models, the *TWI-p.80* model shows greatest predictive skill with a median AUROC of 0.72. However, three of ten folds tested poorly ($<$0.66), which indicates high model uncertainty for predictions of connectivity.

As with the scar-size connectivity models, the greatest variation in effect size is found with *DisOvrlnd* and *VDis* (Fig. A3). The least variation is found in the morphological *TWI-p.90* connectivity model. However, this is explained by the well-balanced dataset of connected to unconnected landslides (Table 2), which means resampling from the unconnected would result in very similar datasets across the 100 model runs compared to the other five targets used. This approach is still meaningful in that it is much like a repeated cross-validation (100 $\times$ 10-fold CV). *DisOvrlnd* is the most important variable for predicting connectivity to *Streams* and, while still important for the TWI-models, its effect is less pronounced. As with the scar-size connectivity models, north-facing slopes are generally more likely to connect to water ways than south-facing slope. This may be due to topographic differences and variation in soil properties that influence properties such as clay content.

3.3. Quantifying reduction of sediment delivery at farm scale

The spatial predictions of landslide connectivity were reclassified into three classes using probability thresholds. These were obtained by ranking all connected scars (Table 2) in descending order and extracting the probability values at the 80th and 95th percentiles. Thus, 80% of scars connecting to streams have probability values $>$0.42 and 95% $>$ 0.25. The probability values were reclassified into three classes describing the likelihood of sediment delivery using these thresholds. The "high" connectivity class represents the area where 80% of connected scars are located; the "moderate" is representative of terrain where 15% of all connected scars were triggered; and finally, the "low" class where the remaining 5% of all connected scars were triggered (Table 3).

Increases in model accuracy increases the refinement of spatial predictions. This has implications from an erosion and sediment mitigation perspective. A connectivity model with poor performance may have large uncertainties in spatial predictions, which reflects in the difficulty to classify units as potentially connected/ unconnected. This in turn increases the proportion of land that requires biological mitigation due to the uncertainty.

A landslide susceptibility or connectivity model with greater accuracy can classify spatial units as stable/unstable or connected/unconnected with much greater certainty. This in turn enables more precise targeting of erosion and sediment mitigation. Observable differences in the spatial predictions of landslide connectivity predictions across the six different morphometric models are thus both functions of varying target definition and inherent model uncertainties (Fig. 9).

Hillslope-channel coupling of landslides is largely dependent on the run-out distance of landslide deposits and the proximity to the connectivity target. The spatial definition of the connectivity target determines the distance landslide-derived material must be transported to enter the channel network. Therefore, the landslide connectivity ratio (LCR), i.e.,

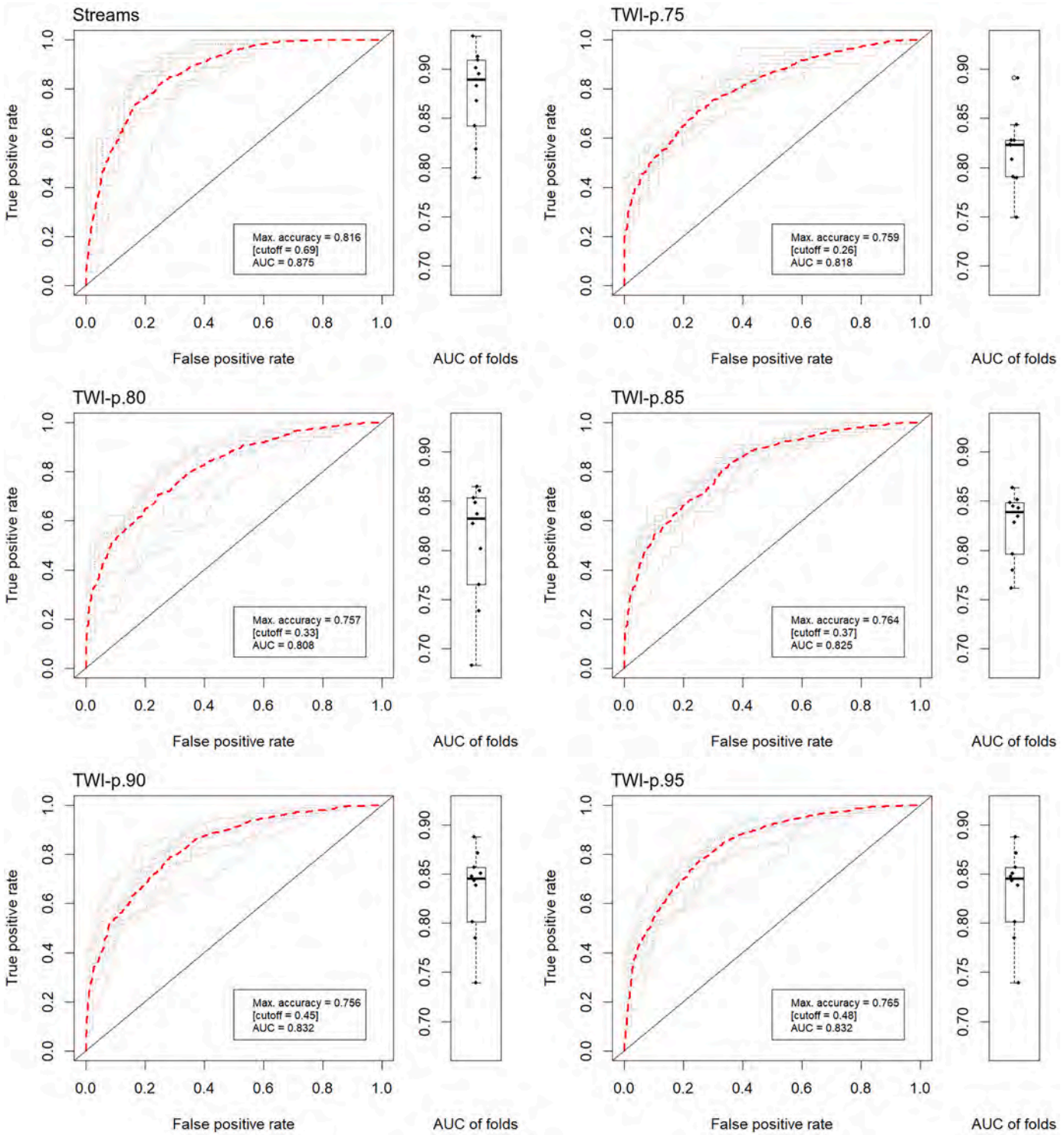

Fig. 6. ROC plots for best of 100 models including scar size variables based on six different connectivity targets. The grey dashed lines are ROC-curves based on validation using 10-fold CV. The red dashed line is the ROC curve based on model predictions of entire unbalanced dataset (2002 scars). Maximum accuracy is calculated using the cut-off that renders the highest accuracy for the entire dataset. Boxplots show the corresponding AUROC values: the box indicates the IQR, whiskers show the minimum and maximum values. (For interpretation of the references to colour in this figure legend, the reader is referred to the web version of this article.)

the proportion of connected landslide scars, is lowest for the 5 m buffered streams (0.27), and highest for the *TWI-p.75* zone (0.69; Table 3). Since the size of connected landslides are on average larger than unconnected scars (Table 2), the SDR does not equal the LCR (Table 3). Further, we assume the proportion of mobilised sediment retained on the hillslope increases for each of the successive connectivity targets.

Estimated SDRs ranges from 0.21 for the *Streams* connectivity target, increasing to 0.29 for the *TWI-p.90* target before dropping back to 0.21 for the TWI-p.75 target. Assuming highly saturated soils enabled surface runoff to continue during and post storm event, sediment delivery was also 21% for the *TWI-p.75* scenario. The highest sediment delivery ratio of 0.29 was found for the *TWI-p.90* scenario.

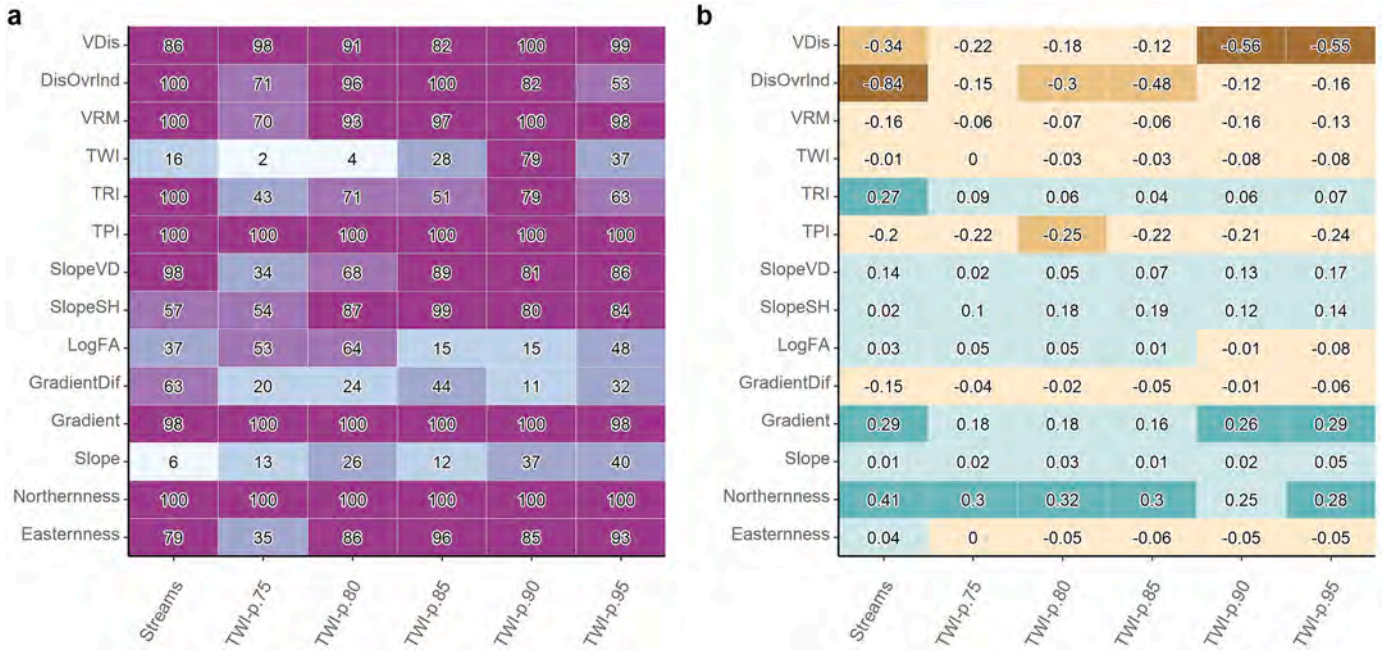

Fig. 7. Insert a): Heat-map displaying the inclusion rate of variables for all 6 connectivity targets excluding the scar size variables. The numbers indicate how often variables were selected for the models out of 100 estimates. Note that the exclusion of scar size variables increases inclusion rate of morphometric variables. Darker colours show variables selected more frequently. Grey box with a dash indicates the variable was never selected for the models. Insert b): Heat-map displaying estimates of coefficients (median of non-zero estimates) for all six connectivity-targets. The grey box is equivalent to a coefficient of zero and was never selected for the models.

Assuming an average scar depth of 1 m and soil with bulk density of 1.4 (Crozier, 1996), the equivalent sediment yield for the 1977 rainfall event was 3548 t/km^2 for the *Streams* connectivity target and 7564 t/km^2 using the *TWI-p.75* connectivity scenario (Table 3). The resulting sediment yield is much greater despite the delivery ratio not changing (0.21 for both Streams and *TWI-p.75*), likely reflecting the larger proportion of landslides connecting to the connectivity target. However, at 9033 t/km^2, the highest sediment yield is found for the *TWI-p.85* scenario. The results suggest sediment yield is a function of the landslide connectivity ratio and the capacity of sediment to be entrained when mobilised material is not delivered directly to the channel network.

3.4. Land management scenario modelling

Scenario modelling across 50 farms (with a median farm size of 608 ha) shows that, under the treeless baseline scenario, only 6.5% (2400 ha) of the total area is both highly susceptible to shallow landsliding and has high potential for sediment delivery to the stream network (Fig. 10a). However, due to the actual tree cover (WV), this class now represents just 4.7% of the total area (Fig. 10b). The change in class distribution from a pasture-only scenario (Fig. 11a) to that of 2013 (Fig. 11b) has led to an estimated reduction in sediment delivery of 23.8% across the 50 farms (Table 4). Targeted mitigation of the 6.5% of highly susceptible and connected land using a 15 × 15 m grid of poplars (Fig. 11c, e) has potential to reduce sediment delivery by 33.6% compared with the baseline scenario. The maximum reduction in sediment delivery using the same 15 m-spaced trees covering all farmland is 56.1%. Under these scenarios, the sediment yield for the storm event of 1977 would have been reduced from 3548 t/km^2 (equivalent to the pasture-only scenario S_0) to 2703 t/km^2 due to actual vegetation (*WV*), 2356 t/km^2 for S_1 (targeted) and 1557 t/km^2 for S_2 (maximum; Table 3).

4. Discussion

4.1. Sediment delivery by landslides

Empirical investigation of runout behaviour, mobility and connectivity of shallow landslides typically includes a quantification of the source material deposited into streams (i.e., the sediment-delivery ratio - SDR). SDRs of shallow landslides can vary significantly and are dependent on soil mass, topography (e.g., slope geometry, surface roughness), soil type (e.g., clay content, saturated water content that produces liquid behaviour in soils) and available zone of accumulation prior to entering a water course (Bathurst et al., 1997; Crozier, 1996; Cislaghi and Bischetti, 2019; Cavalli et al., 2013; Bessette-Kirton et al., 2020). Estimates for sediment delivery ratios can be used to inform process-specific contributions to long-term (e.g., Dymond et al., 2016) or event-scale sediment budgets (e.g., Page et al., 1994).

Reid and Page (2002) investigated connectivity of landslide deposits to streams in the Waipaoa catchment (East Coast of North Island, NZ) and found 65% of landslides connected to streams, with an overall sediment delivery ratio of 0.45. In contrast, Jones and Preston (2012) estimated a sediment delivery ratio ranging from 0.12 to 0.28 in the same catchment. Furthermore, through field measurements, Preston (2008) quantified SDRs ranging between 0.23 and 0.28. These estimates by Jones and Preston (2012) and Preston (2008) are similar to our findings despite the different geomorphological setting (SDR 0.21; Table 3). Empirical investigation during landslide-triggering events and process-based modelling could help alleviate the current paucity of knowledge related to transport capacity of sediment following landslide initiation. In this regard, the timing of landsliding with respect to storm duration is an important consideration in terms of transport capacity during the event (Preston, 2008). The scenarios using TWI-based connectivity targets aim to address this knowledge gap by quantifying SDRs based on assumptions of increased delivery and reworking of the deposited mass during the rainfall event. However, these TWI-based connectivity targets can also be used to characterize potential increases in SDR through surface run-off erosion post-event (Xiong et al.,

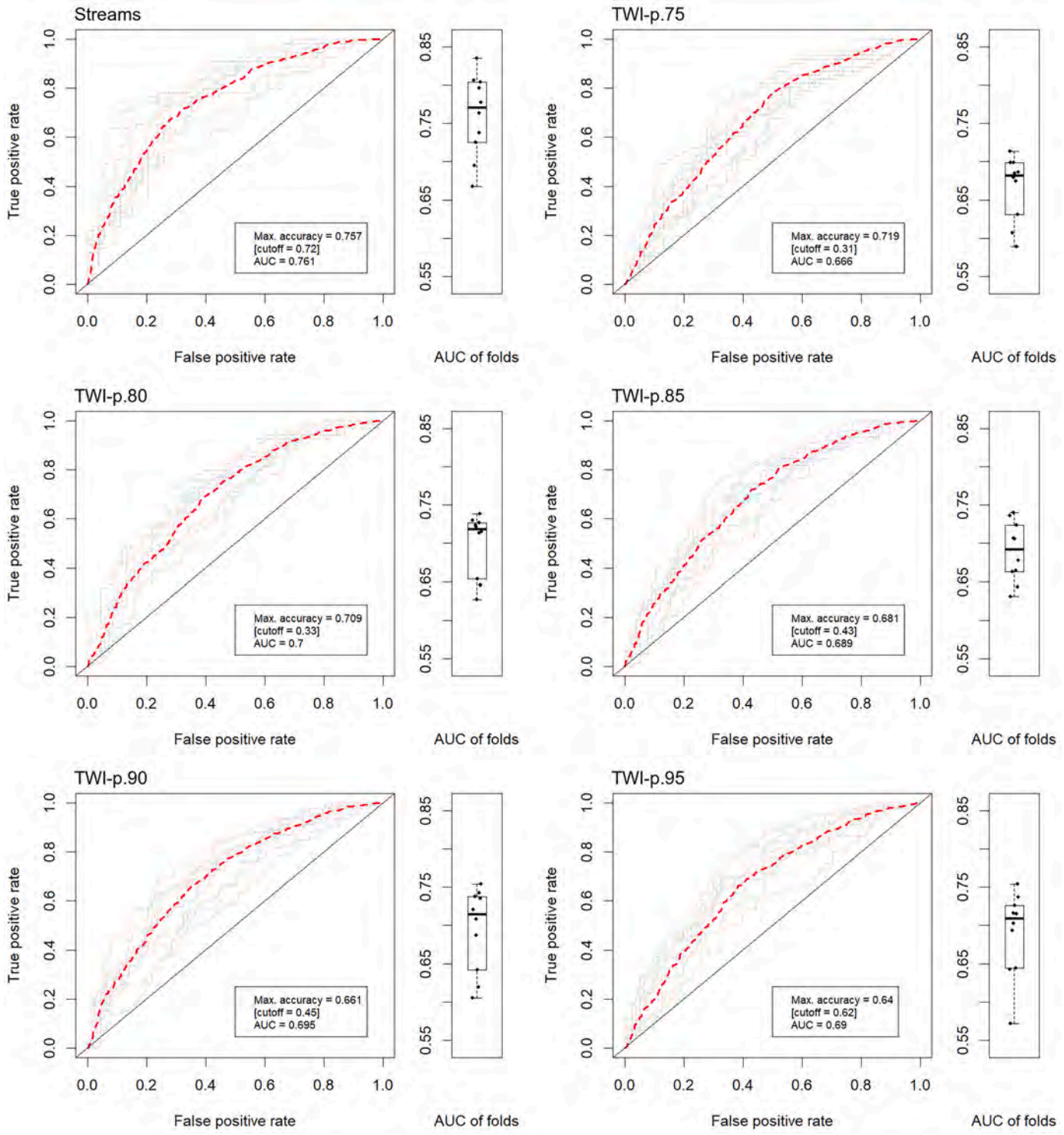

Fig. 8. ROC plots for best of 100 models including only morphometric variables based on six different connectivity targets. The grey dashed lines are ROC-curves based on validation using 10-fold CV. The red dashed line is the ROC curve based on model predictions of entire unbalanced dataset (2002 scars). Maximum accuracy is calculated using the cut-off that renders the highest accuracy for the entire dataset. Boxplots show the corresponding AUROC values: the box indicates the IQR, whiskers show the minimum and maximum values. (For interpretation of the references to colour in this figure legend, the reader is referred to the web version of this article.)

2022). Under these assumptions, our results show the SDR could potentially increase to 0.43 (Table 3). However, field measurements or use of high-resolution repeat LiDAR are required to corroborate these findings (Scheip and Wegmann, 2022).

The SDRs equate to an event sediment yield of between 3548 t km^{-2} and 9033 t km^{-2} (Table 3). To put this into context, the study area drains into the Taueru River, which – based on sediment gauging data – has an average annual sediment yield of 358 t km^{-2} (Hicks et al., 2019). However, this estimate of sediment yield for the Taueru is based on a sediment monitoring period from May 1968 – May 1981 (at Te Weraiti). It therefore includes the effect of the 1977 storm event and subsequent contribution of sediment from landslides, which can impact on sediment

Table 3
Landslide connectivity ratios, landslide delivery ratios, and event sediment yields for the three connectivity classes and six targets.

Connectivity class		Streams	TWI-p.75	TWI-p.80	TWI-p.85	TWI-p.90	TWI-p.95
Landslide connectivity ratio	Low	0.01	0.03	0.03	0.03	0.03	0.02
	Medium	0.04	0.10	0.10	0.09	0.08	0.06
	High	0.22	0.55	0.52	0.49	0.43	0.32
	Total	0.27	0.69	0.65	0.61	0.54	0.40
Sediment delivery ratio	Low	0.01	0.01	0.01	0.02	0.02	0.01
	Medium	0.04	0.03	0.03	0.05	0.06	0.04
	High	0.16	0.18	0.20	0.21	0.21	0.21
	Total	0.21	0.21	0.25	0.28	0.29	0.26
Event sediment yield(t/km^2)	Low	383	1299	1711	2237	2298	1068
	Medium	2771	3605	4412	6522	6799	3742
	High	6564	13,527	13,620	13,885	12,568	8523
	Total	3548	7564	8366	9033	8545	6027

loads for several years (Basher et al., 2011). Even so, by comparing the event sediment yields (Table 3) with average annual estimates, it is evident that shallow landslides are the dominant source of sediment in the Taueru Catchment. Multi-temporal mapping in the same study area confirms that landsliding is a regular occurrence in these landscapes: Over the course of 128 years (1882–2010), the cumulative scar area comprised 22% of the planform area of the study site (60 ha), which equates to 2% of the land surface per decade (De Rose, 2013).

The relative importance of shallow landslides to long-term sediment loads can differ significantly – even within the same catchment (Hicks et al., 2000). Shallow landsliding was found to be the dominant erosion process in the Te Arai sub-catchment (Hicks et al., 2000), which comprises 23% of the Waipaoa Catchment. However, for the Waipaoa Catchment as a whole, landslides contribute only about 15 ± 5% of the long-term suspended sediment load in the Waipaoa River (Reid and Page, 2002) – increasing to ~48% during extreme events (Page et al., 1999). Other erosion processes in other parts of the catchment are more significant sediment sources (Hicks et al., 2000; Reid and Page, 2002), particularly the extensive gully systems (Marden et al., 2018), but also streambank erosion (De Rose and Basher, 2011). Landslides were also determined to be the most important contributor to the sediment load of the Manawatū catchment (Dymond et al., 2016). However, such estimates are very sensitive to the universal SDR used (0.50), which is known to vary depending on morphological setting (Dickinson and Wall, 1977). Indeed, Burns (1979) suggested that each potential sediment source has unique delivery potential, which can be quantified in terms of probability with respect to the stream and catchment divide. Our approach overcomes these limitations by having developed statistical connectivity models using a suite of morphometric variables to predict the likelihood of a landslide delivering sediment to a predefined sink and can therefore be considered an integration of functional and structural connectivity (Najafi et al., 2021a). Yet, how the predictions translate into SDRs requires further research but could be based on an empirical relationship between probability values of landslide connectivity and observed estimates of SDR. While the model is limited by the landslide inventory which characterises a single event for a 7-km^2 area, future development will also aim to increase the landslide scar-deposit inventory so that soil characteristics (e.g., texture) can be included in the model. In addition, it would be important to determine sensitivity of predicted reductions in landslide susceptibility and connectivity to the choice of statistical model (e.g., a generalised additive model or a random forest model).

The scenarios presented here are based on past observations of both landslide occurrence from the years 2005–2010 and sediment delivery from the 1977 event. Predicted rates of sediment delivery and reductions associated with actual tree cover and mitigation scenarios compared to a pasture baseline assume the mechanisms of failure and delivery will be similar in future. Validation of the landslide susceptibility model shows a shift in terms of probability distribution of the 1977 landslide inventory compared with the larger, more recent landslide inventory from 2005 to 2009 used to generate the susceptibility model (Fig. 12). Only 70.5% of landslides triggered in 1977 are located in the high susceptible class. The high class used for scenario modelling is defined by a probability threshold of 0.72 that represents the 80th percentile of landslide scars ranked in descending order in the landslide inventory of 2005–2009. By extracting the landslide susceptibility values at the scar locations from 1977, the equivalent 80th percentile probability threshold of 1977 landslide scars is 0.60. The results of the validation suggest that historic landslides were occurring more frequently on what is considered “moderately susceptible terrain” by a present-day susceptibility model. This may reflect differences in the triggering mechanism, that is, long-duration (low-intensity) rainfall with high antecedent conditions in 1977 versus the high intensity rainfall events of 2005–2009 (Crozier et al., 1980; Spiekermann et al., 2021). However, it may also be an indication of terrain resistance (Crozier and Preston, 1999; Jones and Preston, 2012). The location of more recent failures likely reflects the erosional history of the landscape where undisturbed regolith close to spurs and crests has little lateral support due to previous failures lower on the slope (Preston, 2008). Topographic controls on surface and sub-surface flow and water content not only impact landslide occurrence, but also have implications for the behaviour of debris runout. As the landslide mass proceeds downslope, its mobility will increase due to greater surface water flows resulting from convergence in flow paths and larger drainage area. This has the effect of increasing the liquid fraction of the landslide deposit, which reduces internal friction, resulting in greater run-out down-slope (Scheip and Wegmann, 2022). If, because of terrain event resistance (Jones and Preston, 2012), landslide failures are occurring increasingly on steeper upper slopes, the likelihood of fluidised flow may be reduced due to lower soil water content in these areas of initiation. In addition, results show the importance of landslide density in determining sediment delivery, and in this regard are similar to findings elsewhere (e.g., Bessette-Kirton et al., 2020). Landslide deposits formed from multiple source areas that coalesce were more likely to deliver to the stream network than single source landslide deposits. Further research is needed to examine the relationship between i) landslide-triggering rainfall magnitude, ii) topographic controls on landslide initiation, iii) evolution of terrain resistance, and iv) type of debris runout, i.e., fluidised with internal friction removed, intact sliding of a landslide mass or incipient failure.

4.2. Smarter targeting of erosion and sediment mitigation

Scenario modelling results provide clear evidence that the cost-effectiveness of targeted mitigation S_1 is greatly increased compared to a non-targeted approach. A targeted approach involves prioritizing mitigation on slopes with high landslide susceptibility and high potential for sediment delivery. On average, just 3 trees/ha of farm are required to mitigate the 2400 ha of highly susceptible and connected terrain across the 50 farms. The median area of this zone requiring mitigation is 36 ha across the 50 farms, which would require an investment of approximately $53,000 to achieve the median reduction of

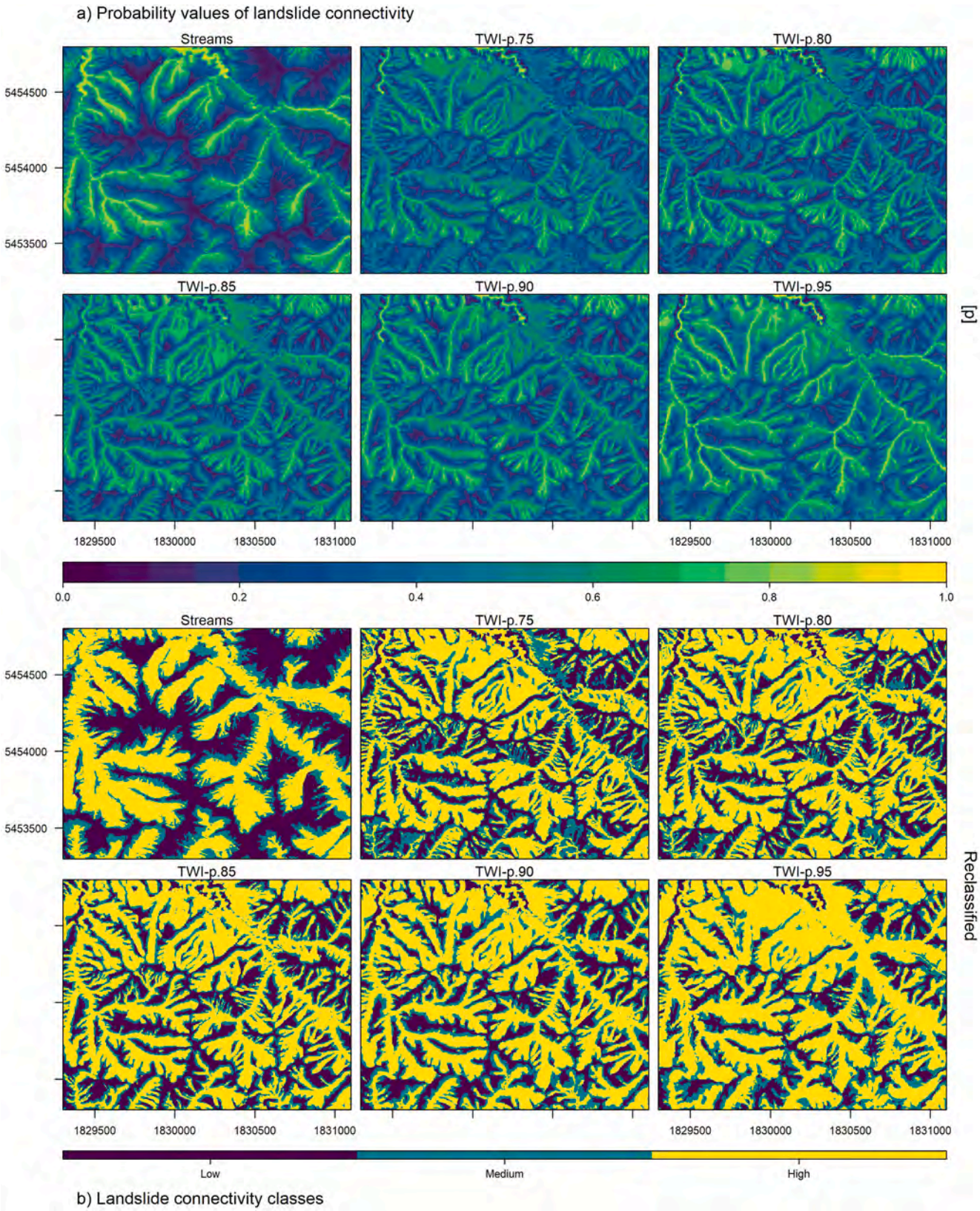

Fig. 9. a) For a sample area (1800 m by 1500 m), probability values of connectivity and b) reclassified connectivity into three classes expressing the likelihood of sediment delivery according to the probability distribution of connected scars (see Fig. A4). Projection: New Zealand Transverse Mercator 2000 (NZTM2000).

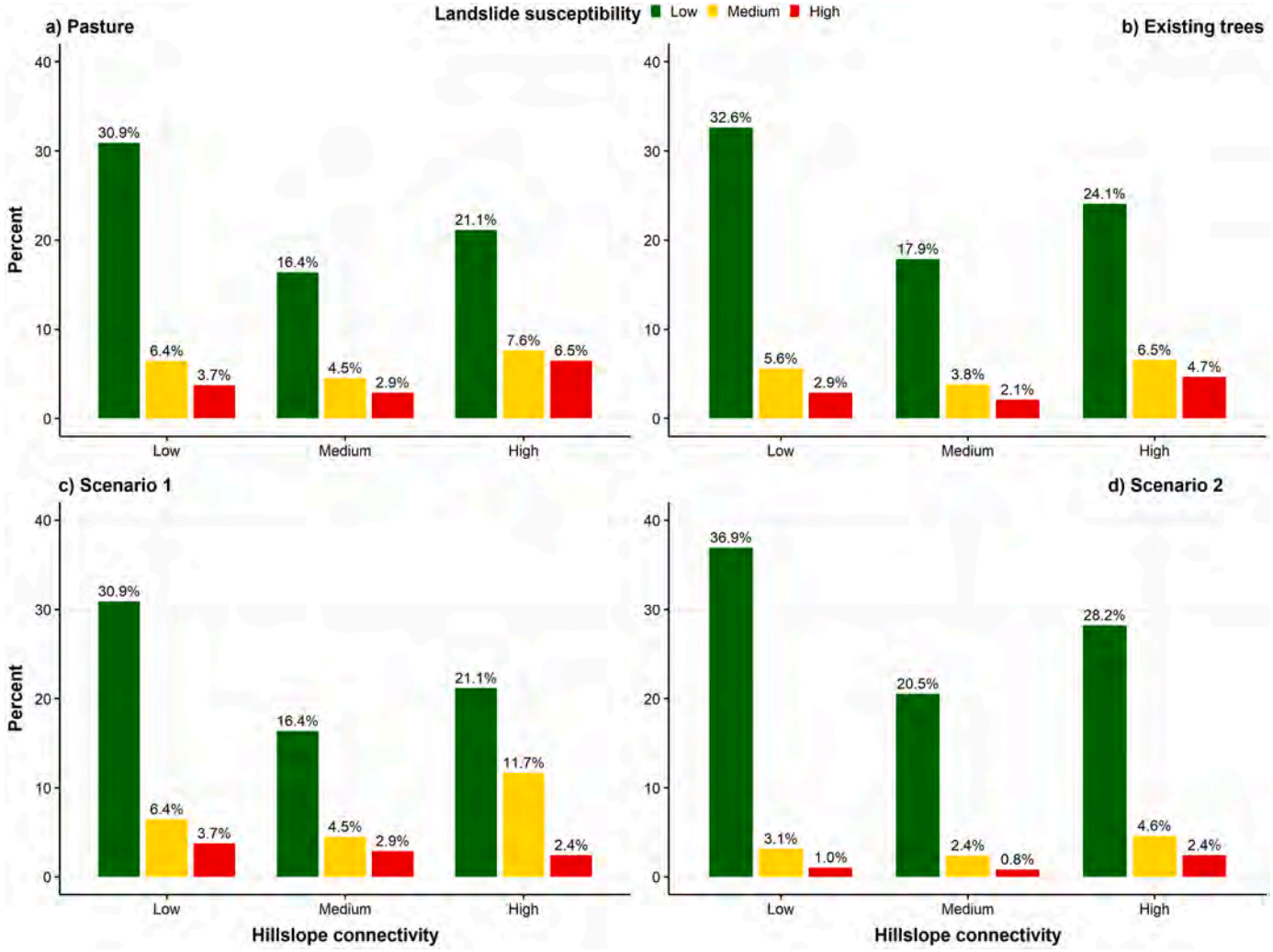

Fig. 10. Landslide susceptibility and connectivity distribution of combined farms (total area 36,500 ha).

33.6%. Thus, the average investment required on a per hectare basis amounts to $2.82 per 1% reduction in sediment delivery from shallow landslides. This compares to S_2, which represents a random approach to targeting, i.e., mitigation is implemented proportional to the area occupied by the landslide susceptibility/connectivity classes. The average investment to achieve a 1% reduction in sediment delivery is thus substantially greater ($26.2/ha).

For example, if a 10% reduction is desired (compared to baseline) for a 500-ha farm, the investment would amount to $14,100 – assuming all trees survive. To achieve a 10% reduction on the same farm using a non-targeted approach, an investment of approximately $131,000 would be required. There is thus an order of magnitude difference in terms of cost-effectiveness between a targeted versus non-targeted approach. However, it is important to consider the variation in terms of reduction in sediment delivery achieved and the cost of doing so across the 50 farms (Fig. 13). The mean cost for a 1% reduction is $2.82/ha for Scenario 1 (SD: $1.37; range: $0.21–$7.92); The mean for Scenario 2 is $26.20/ha (SD: 3.69; range: $17.54 – $38.94).

Due to the actual tree cover in the Wairarapa hill country, sediment delivery from shallow landsliding is 23.8% less, compared with a pasture-only scenario. In fact, the importance of already existing vegetation is similar to what could be achieved using a targeted approach (33.6% reduction). However, the estimated number of trees in the landscape is substantially different. Approximately 34% of land across the 50 properties have added protection due to the presence of trees. However, many of these trees are not providing a direct benefit in terms of slope stability (e.g., when located on floodplains), but are likely adding value to the farm enterprise elsewhere (e.g., through shelter provision, additional income from honey, carbon, or forestry). In terms of future erosion and sediment control works, the cost-effectiveness is substantially increased by targeting highly susceptible and connected slopes.

5. Conclusion and outlook

This study developed and tested statistical approaches to modelling sediment mobility from shallow landslides by coupling slope stability and sediment connectivity models. The method demonstrates a useful integration of functional and structural connectivity. We have demonstrated the development and application of the first morphometric connectivity model to enable targeted mitigation of landslide-derived sediment. The model has very limited data requirements: 1) an inventory of landslide scars and deposits and 2) a high-resolution (LiDAR) DEM. An important outcome of the lasso regression is the potential consequence of over-reliance on individual landslide scar size as a predictor of connectivity. Without considering contributions of landslide-derived material from multiple sources to the transport of delivery downslope, the run-out distance is likely to be underestimated for shallow landslides. This result speaks in favour of a morphometric model given the difficulty in predicting the location, size, and density of future

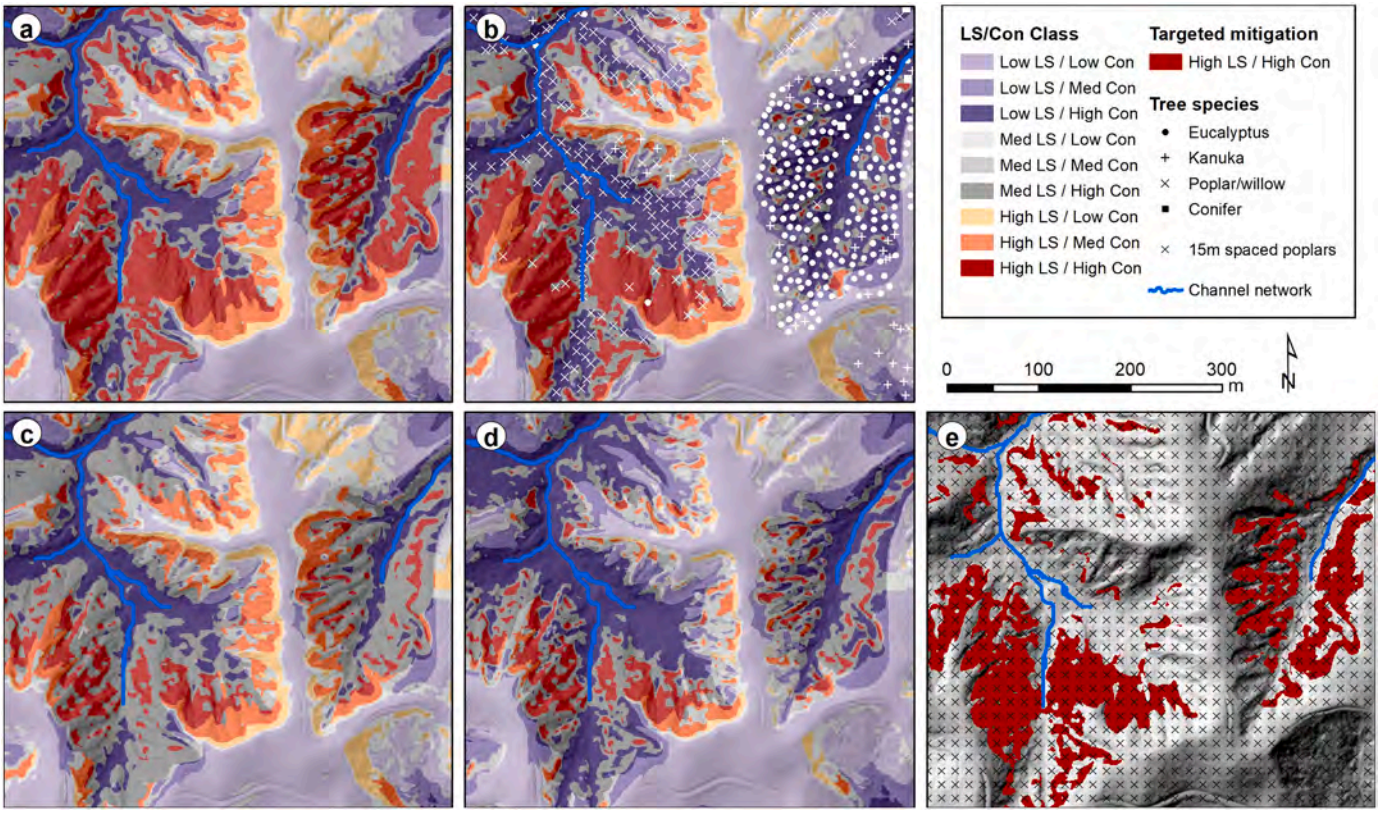

Fig. 11. Landslide susceptibility and connectivity maps under a) pasture, b) actual tree cover (2013), c) targeted mitigation to terrain shown in e), and d) full tree cover using 15 × 15 m grid of poplar trees shown in e).

Table 4
Overall reduction in sediment delivery to streams across 50 farms (35,900 ha) relative to baseline (S0).

	Existing vegetation	Scenario 1	Scenario 2
Reduction (%)	23.8	33.6	56.1
Tree count	738,818	105,307	1,629,381
Area treated (ha)	12,480	2369	36,661
Farm-average trees/ha	20.2	2.9	44.4
Average cost for 1% reduction ($/ha)	na	2.82	26.2

shallow landslides. However, removal of scar size variables comes at a cost in terms of model performance. For the *Streams* connectivity model, the median AUROC was reduced from 0.88 to 0.75 across 100 repetitions.

To simulate the variation in sediment delivery based on a range in storm magnitude, we defined six different sediment connectivity targets. Sediment delivery ratios from the landslide triggering event of 1977 ranged between 0.21 and 0.29, depending on the definition of sink. However, the connectivity scenarios show that sediment yields can change significantly depending on the degree to which sediment recruitment from lower slopes is possible during a storm event. When accounting only for direct deposition into streams, the event sediment

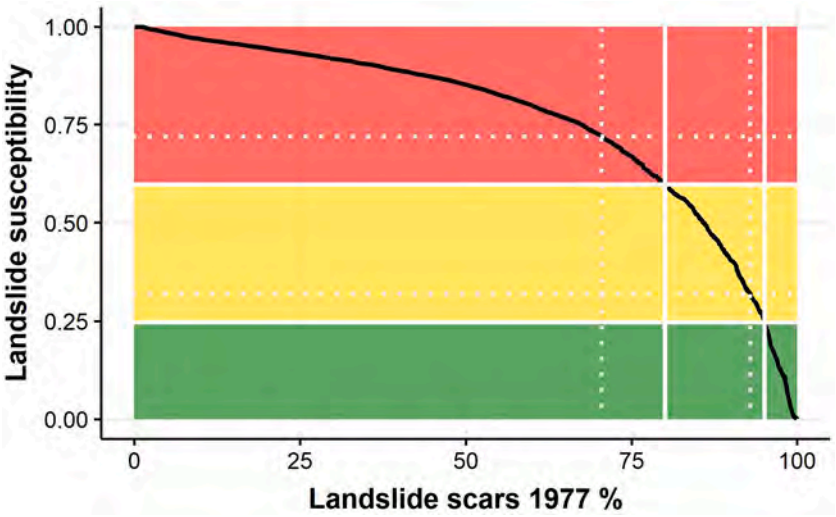

Fig. 12. Validation of the landslide susceptibility model based on historic landslides. White lines locate the probability thresholds at the 80th and 95th percentiles in the count of landslides ranked in descending order according to landslide susceptibility values. Dotted lines show the cut-offs used to classify landslide susceptibility into three classes of Low, Medium, and High susceptibility according to the probability distribution in the landslide inventory from 2005 to 2009 (Spiekermann et al., 2022).

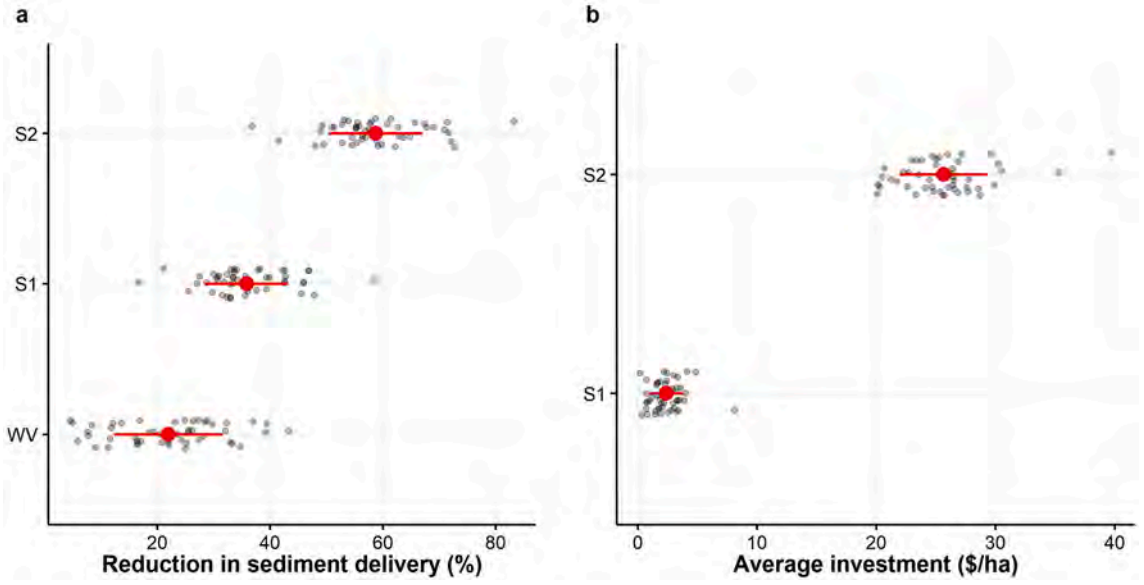

Fig. 13. Insert a). Modelled reduction in sediment delivery to the stream network (%) for actual woody vegetation (WV; 2013), targeted mitigation (S1) and maximum possible with full tree cover (S2). Red strip charts correspond to the mean of sediment reductions (point) from 50 farms and 1 SD (line); Insert b). The farm-average investment required on a per hectare basis to achieve a 1% reduction in sediment delivery. (For interpretation of the references to colour in this figure legend, the reader is referred to the web version of this article.)

yield was estimated at 3548 t/km^2 (Table 3). However, when assuming continued sediment recruitment at reduced rate by overland flow across saturated soils as well as post-event reworking of deposited material, the maximum sediment yield was estimated at 9033 t/km^2. This estimate of event sediment yield is approximately 2.5 times greater than estimates only considering landslide deposits connecting to streams directly and challenges previous assumptions related to sediment delivery ratios and the importance of shallow landsliding for sediment budgets.

We selected 50 farms to quantify the reduction in sediment delivery based on contrasting mitigation options: 1) targeting critical source areas of sediment and 2) a non-targeted approach to tree planting. The cost-effectiveness of these different mitigation options suggests there is an order of magnitude difference between a targeted versus non-targeted approach in terms of the ratio of investment to reduction in sediment delivery achieved. An important outcome of the landslide susceptibility and connectivity modelling is that in total only 6.5% (2370 ha) of farmland is the potential source of approximately two-thirds of landslide-derived sediment across the 50 farms (Fig. 11). Due to existing vegetation, this area has already been reduced to 4.7% (1720 ha). Further reductions in future sediment delivery can be achieved by increasing slope stability on these highly susceptible and connected slopes through additional biological mitigation. For a farm of 500 ha, the average cost to achieve a 10% reduction in landslide-derived sediment is $14,100 for targeted mitigation and $131,000 for non-targeted (Table 4). To achieve the maximum reduction possible for a targeted approach to mitigation using a 15-m grid of poplar poles on the same farm (500 ha), the cost is estimated as $47,000 for targeted mitigation and $440,000 for non-targeted to achieve the same result of 33.6% reduction in sediment delivery. However, further research is required to test the feasibility of treatment across different landslide susceptibility classes. Shallow landslides are more likely to occur on steep slopes where establishment of biological controls (e.g., poplar poles) is more challenging due to reduced soil moisture, exposure to wind gusts, and shallower soils.

In terms of future research needs, increasing landslide scar-deposit inventories across a range of environments could allow statistical connectivity models to include soil characteristics (e.g., soil type, depth, etc.). Furthermore, there is currently a lack of understanding regarding the relationship between triggering mechanism, topographic controls, and terrain resistance (Jones and Preston, 2012) and debris run-out behaviour of shallow landslides. Our results show that both scar size and the density of landslide occurrence are very important as determinants of sediment delivery since coalescing landslide deposits are much more likely to deliver sediment, which is corroborated by related research (e.g., Scheip and Wegmann, 2022). Therefore, future landslide susceptibility models should provide predictions on the intensity of landslides (Lombardo et al., 2018, 2020), their size (Lombardo et al., 2021) and probability of landslide deposits coalescing. While the morphometric connectivity model was developed to support land management decisions and increase effectiveness of erosion and sediment mitigation, there is equally great potential to include the spatial predictions of connectivity in sediment budget modelling at catchment scale.

CRediT authorship contribution statement

Raphael I. Spiekermann: Conceptualization, Data curation, Methodology, Software, Validation, Formal analysis, Investigation, Writing – original draft, Visualization. **Hugh G. Smith:** Conceptualization, Supervision, Writing – review & editing. **Sam McColl:** Supervision, Writing – review & editing. **Lucy Burkitt:** Supervision, Writing – review & editing. **Ian C. Fuller:** Supervision, Writing – review & editing.

Declaration of Competing Interest

The authors declare that they have no known competing financial interests or personal relationships that could have appeared to influence the work reported in this paper.

Acknowledgements

This research was supported by New Zealand Ministry of Business, Innovation and Employment research program “Smarter Targeting of Erosion Control (STEC)” (Contract C09X1804) and the Strategic Science Investment Fund (SSIF) allocated to Manaaki Whenua – Landcare Research.

Appendix A. Supplementary data

Supplementary data to this article can be found online at https://doi.org/10.1016/j.ecoleng.2022.106676.

References

Akalin, A., Franke, V., Uyar, B., Ronen, J., 2020. Computational Genomics with R. Berlin, Germany. https://compgenomr.github.io/book/.

Basher, L.R., 2013. Erosion Processes and their Control in New Zealand. In: Dymond, J.R. (Ed.), Ecosystem Services in New Zealand – Conditions and Trends. Manaaki Whenua Press, Lincoln, New Zealand, pp. 363–374.

Basher, L.R., Hicks, D.M., Clapp, B., Hewitt, T., 2011. Sediment yield response to large storm events and forest harvesting, Motueka River, New Zealand. New Zeal. J. Mar. Freshw. Res. 45, 333–356. https://doi.org/10.1080/00288330.2011.570350.

Basher, L., Betts, H., Lynn, I., Marden, M., McNeill, S., Page, M., Rosser, B., 2018. A preliminary assessment of the impact of landslide, earthflow, and gully erosion on soil carbon stocks in New Zealand. Geomorphology 307, 93–106. https://doi.org/10.1016/j.geomorph.2017.10.006.

Basher, L., Spiekermann, R., Dymond, J., Herzig, A., Hayman, E., Ausseil, A.G., 2020. Modelling the effect of land management interventions and climate change on sediment loads in the Manawatū–Whanganui region. New Zeal. J. Mar. Freshw. Res. 54, 490–511. https://doi.org/10.1080/00288330.2020.1730413.

Bathurst, J.C., Burton, A., Ward, J.T., 1997. Debris flow run-out and landslide sediment delivery model tests. J. Hydraul. Eng. 123, 410–419. https://doi.org/10.1061/(ASCE)0733-9429(1997)123:5(410).

Bellugi, D., Milledge, D.G., Dietrich, W.E., McKean, J.A., Perron, J.T., Sudderth, E.B., Kazian, B., 2015a. A spectral clustering search algorithm for predicting shallow landslide size and location: a shallow landslide search algorithm. J. Geophys. Res. Earth Surf. 120, 300–324. https://doi.org/10.1002/2014JF003137.

Bellugi, D., Milledge, D.G., Dietrich, W.E., Perron, J.T., McKean, J., 2015b. Predicting shallow landslide size and location across a natural landscape: application of a spectral clustering search algorithm. J. Geophys. Res. Earth Surf. 120, 2552–2585. https://doi.org/10.1002/2015JF003520.

Benavides, R., Douglas, G.B., Osoro, K., 2009. Silvopastoralism in New Zealand: Review of effects of evergreen and deciduous trees on pasture dynamics. Agrofor. Syst. 76, 327–350. https://doi.org/10.1007/s10457-008-9186-6.

Bessette-Kirton, E.K., Coe, J.A., Schulz, W.H., Cerovski-Darriau, C., Einbund, M.M., 2020. Mobility characteristics of debris slides and flows triggered by Hurricane Maria in Puerto Rico. Landslides 17, 2795–2809. https://doi.org/10.1007/s10346-020-01445-z.

Betts, H., Basher, L., Dymond, J., Herzig, A., Marden, M., Phillips, C., 2017. Development of a landslide component for a sediment budget model. Environ. Model. Softw. 92, 28–39. https://doi.org/10.1016/j.envsoft.2017.02.003.

Böhner, J., Selige, T., 2006. Jürgen Böhner 1 & Thomas Selige 2 1 115, pp. 13–28.

Borselli, L., Cassi, P., Torri, D., 2008. Prolegomena to sediment and flow connectivity in the landscape: a GIS and field numerical assessment. Catena 75, 268–277. https://doi.org/10.1016/j.catena.2008.07.006.

Bracken, L.J., Turnbull, L., Wainwright, J., Bogaart, P., 2015. Sediment connectivity: a framework for understanding sediment transfer at multiple scales. Earth Surf. Process. Landf. 40, 177–188. https://doi.org/10.1002/esp.3635.

Brenning, A., 2005. Spatial prediction models for landslide hazards: Review, comparison and evaluation. Nat. Hazards Earth Syst. Sci. 5, 853–862. https://doi.org/10.5194/nhess-5-853-2005.

Brenning, A., Bangs, D., Becker, M., 2018. RSAGA: SAGA Geoprocessing and Terrain Analysis. R Package Version 1.3.0. https://CRAN.R-project.org/package=RSAGA.

Brierley, G., Fryirs, K., Jain, V., 2006. Landscape connectivity: the geographic basis of geomorphic applications. Area 38, 165–174. https://doi.org/10.1111/j.1475-4762.2006.00671.x.

Broeckx, J., Vanmaercke, M., Bălteanu, D., Chendeş, V., Sima, M., Enciu, P., Poesen, J., 2016. Linking landslide susceptibility to sediment yield at regional scale: application to Romania. Geomorphology 268, 222–232. https://doi.org/10.1016/j.geomorph.2016.06.012.

Burns, R.G., 1979. An improved sediment delivery model for Piedmont forests. In: Environ- Mental Resource Centre Annual Report. Georgia Institute of Technology, Atlanta, USA, pp. 379–382.

Burton, A., Bathurst, J.C., 1998. Physically based modelling of shallow landslide sediment yield at a catchment scale. Environ. Geol. 35, 89–99. https://doi.org/10.1007/s002540050296.

Cavalli, M., Trevisani, S., Comiti, F., Marchi, L., 2013. Geomorphometric assessment of spatial sediment connectivity in small Alpine catchments. Geomorphology 188, 31–41. https://doi.org/10.1016/j.geomorph.2012.05.007.

Cislaghi, A., Bischetti, G.B., 2019. Source areas, connectivity, and delivery rate of sediments in mountainous-forested hillslopes: a probabilistic approach. Sci. Total Environ. 652, 1168–1186. https://doi.org/10.1016/j.scitotenv.2018.10.318.

Corominas, J., 1996. The angle of reach as a mobility index for small and large landslides. Can. Geotech. J. 33, 260–271. https://doi.org/10.1139/t96-005.

Croke, J., Fryirs, K., Thompson, C., 2013. Channel-floodplain connectivity during an extreme flood event: Implications for sediment erosion, deposition, and delivery. Earth Surf. Process. Landf. 38, 1444–1456. https://doi.org/10.1002/esp.3430.

Crozier, M.J., 1996. Runout behaviour of shallow, rapid earthflows. Zeitschrift für Geomorphologie. Suppl.-Bd. 105, 35–48.

Crozier, M.J., 2018. Reprint of "A proposed cell model for multiple-occurrence regional landslide events: Implications for landslide susceptibility mapping.". Geomorphology 307, 3–11. https://doi.org/10.1016/j.geomorph.2018.02.001.

Crozier, M.J., Preston, N.J., 1999. Modelling changes in terrain resistance as a component of landform evolution in unstable hill country. In: Hergarten, S., Neugebauer, H.J. (Eds.), Process Modelling and Landform Evolution, Lecture Notes in Earth Sciences, Vol. 78. Springer, Berlin/Heidelberg/New York, pp. 267–284.

Crozier, M.J., Eyles, R.J., Crozier, M.J., McConchie, J.A., Owen, R.C., 1980. Distribution of landslips in the Wairarapa hill country. New Zeal J. Geol. Geophys. 23, 575–586. https://doi.org/10.1080/00288306.1980.10424129.

Cruden, D.M., Varnes, D.J., 1996. Chapter 3 Landslide types and processes. In: Landslides Investig. Mitigation, Transp. Res. Board Spec. Rep. 247, Washington D.C, pp. 36–75.

Davies-Colley, R.J., 2013. River water quality in New Zealand: an introduction and overview. River Water. Qual. 432–447.

De Rose, R.C., 2013. Slope control on the frequency distribution of shallow landslides and associated soil properties, North Island. New Zealand Earth Surf. Proc. Landforms 38, 356–371. https://doi.org/10.1002/esp.3283.

De Rose, R.C., Basher, L.R., 2011. Measurement of river bank and cliff erosion from sequential LIDAR and historical aerial photography. Geomorphology 126, 132–147. https://doi.org/10.1016/j.geomorph.2010.10.037.

De Walque, B., Degré, A., Maugnard, A., Bielders, C.L., 2017. Artificial surfaces characteristics and sediment connectivity explain muddy flood hazard in Wallonia. Catena 158, 89–101. https://doi.org/10.1016/j.catena.2017.06.016.

Dickinson, W.T., Wall, G.J., 1977. The relationship between source-area erosion and sediment yield. Hydrol. Sci. Bull. 22, 527–530.

Doody, D.G., Archbold, M., Foy, R.H., Flynn, R., 2012. Approaches to the implementation of the Water Framework Directive: Targeting mitigation measures at critical source areas of diffuse phosphorus in Irish catchments. J. Environ. Manag. 93, 225–234. https://doi.org/10.1016/j.jenvman.2011.09.002.

Dunnington, D., 2021. qgisprocess: Use 'QGIS' Processing Algorithms. R Package Version 0.0.0.9000. In: https://github.com/paleolimbot/qgisprocess.

Dymond, J.R., Ausseil, A.-G., Shepherd, J.D., Buettner, L., 2006. Validation of a region-wide model of landslide susceptibility in the Manawatu–Wanganui region of New Zealand. Geomorphology 74, 70–79. https://doi.org/10.1016/j.geomorph.2005.08.005.

Dymond, J.R., Herzig, A., Basher, L., Betts, H.D., Marden, M., Phillips, C.J., Ausseil, A.G. E., Palmer, D.J., Clark, M., Roygard, J., 2016. Development of a New Zealand SedNet model for assessment of catchment-wide soil-conservation works. Geomorphology 257, 85–93. https://doi.org/10.1016/j.geomorph.2015.12.022.

Dymond, J.R., Davies-Colley, R.J., Hughes, A.O., Matthaei, C.D., 2017. Predicting improved optical water quality in rivers resulting from soil conservation actions on land. Sci. Total Environ. 603–604, 584–592. https://doi.org/10.1016/j.scitotenv.2017.06.116.

El Khouli, R.H., Macura, K.J., Barker, P.B., Habba, M.R., Jacobs, M.A., Bluemke, D.A., 2009. Relationship of temporal resolution to diagnostic performance for dynamic contrast enhanced MRI of the breast. J. Magn. Reson. Imaging 30, 999–1004. https://doi.org/10.1002/jmri.21947.

Friedman, J., Hastie, T., Tibshirani, R., 2010. Regularization paths for generalized linear models via coordinate descent. J. Stat. Softw. 33 (1), 1–22. URL. https://www.jstatsoft.org/v33/i01/.

Fuller, I.C., Death, R.G., 2018. The science of connected ecosystems: what is the role of catchment-scale connectivity for healthy river ecology? L Degrad Dev 29, 1413–1426. https://doi.org/10.1002/ldr.2903.

Fuller, I.C., Rutherfurd, I.D., 2021. Geomorphic responses to Anthropogenic Land-Cover Change in Australia and New Zealand. In: Reference Module in Earth Systems and Environmental Sciences. Elsevier. https://doi.org/10.1016/B978-0-12-818234-5.00104-8.

Geertsema, M., Schwab, J.W., Jordan, P., Millard, T.H., Rollerson, T.P., 2010. Chapter 8 Hillslope Processes. In: Pike, R., et al. (Eds.), Compendium of Forest Hydrology and Geomorphology in British Columbia. Land Manag, Handb, p. 66.

Glade, T., 2003. Landslide occurrence as a response to land use change: a review of evidence from New Zealand. Catena 51, 297–314. https://doi.org/10.1016/S0341-8162(02)00170-4.

Guisan, A., Weiss, S.B., Weiss, A.D., 1999. GLM versus CCA spatial modeling of plant species distribution. Plant Ecol. 143 (1), 107–122. https://doi.org/10.1023/A:1009841519580.

Haralick, R.M., 1983. Ridges and valleys on digital images. In: Comput. Vision, Graph Image Process, 22, pp. 28–38. https://doi.org/10.1016/0734-189X(83)90094-4.

Hastie, T., Tibshirani, R., Friedman, J., 2009. The Elements of Statistical Learning – Data Mining, Inference, and Prediction, 2. http://www.springerlink.com/index/D7X7KX6772HQ2135.pdf.

Heckmann, T., Schwanghart, W., 2013. Geomorphic coupling and sediment connectivity in an alpine catchment - Exploring sediment cascades using graph theory. Geomorphology 182, 89–103. https://doi.org/10.1016/j.geomorph.2012.10.033.

Heckmann, T., Vericat, D., 2018. Computing spatially distributed sediment delivery ratios: inferring functional sediment connectivity from repeat high-resolution digital elevation models. Earth Surf. Process. Landf. 43, 1547–1554. https://doi.org/10.1002/esp.4334.

Hicks, D.M., Gomez, B., Trustrum, N.A., 2000. Erosion thresholds and suspended sediment yields, Waipaoa River Basin. New Zealand Water Resour. Res. 36, 1129–1142. https://doi.org/10.1029/1999WR900340.

Hicks, D.M., Shankar, U., Mckerchar, A.I., Basher, L., Lynn, I., Page, M., Jessen, M., 2011. Suspended sediment yields from New Zealand rivers. J. Hydrol. New. Zeal. 50, 81–142.

Hicks, M., Semademi-Davies, A., Haddadchi, A., Shankar, U., Plew, D., 2019. Updated sediment load estimator for New Zealand. NIWA Client Report No. 2018341CH,

prepared for Ministry for the Environment. January 2019. Available online: https://environment.govt.nz/publications/updated-sediment-load-estimator-for-new-zealand/.
Hijmans, R.J., 2021. raster: Geographic Data Analysis and Modeling. R package version 3.4-13. https://CRAN.R-project.org/package=raster.
Hjerdt, K.N., Mcdonnell, J.J., Seibert, J., Rodhe, A., 2004. A new topographic index to quantify downslope controls on local drainage, 40, pp. 1–6. https://doi.org/10.1029/2004WR003130.
Hosmer, D.W., Lemeshow, S., 2000. Applied Logistic Regression. Wiley, New York, NY.
Jia, G., Alvioli, M., Gariano, S.L., Marchesini, I., Guzzetti, F., Tang, Q., 2021. A global landslide non-susceptibility map. Geomorphology 389, 107804. https://doi.org/10.1016/j.geomorph.2021.107804.
Jones, K.E., Preston, N.J., 2012. Spatial and temporal patterns of off-slope sediment delivery for small catchments subject to shallow landslides within the Waipaoa catchment, New Zealand. Geomorphology 141–142, 150–159. https://doi.org/10.1016/j.geomorph.2011.12.037.
Kasai, M., Yamada, T., 2019. Topographic effects on frequency-size distribution of landslides triggered by the Hokkaido Eastern Iburi Earthquake in 2018. Earth, Planets Sp 71. https://doi.org/10.1186/s40623-019-1069-8.
Kopecký, M., Macek, M., Wild, J., 2021. Topographic Wetness Index calculation guidelines based on measured soil moisture and plant species composition. Sci. Total Environ. 757 https://doi.org/10.1016/j.scitotenv.2020.143785.
Kuhn, M., 2020. Caret: Classification and Regression Training. R Package Version 6.0-86. https://CRAN.R-project.org/package=caret.
Lambert, M.G., Trustrum, N.A., Costall, D.A., 1984. Effect of soil slip erosion on seasonally dry wairarapa hill pastures. New Zeal. J. Agric. Res. 27, 57–64. https://doi.org/10.1080/00288233.1984.10425732.
Lilburne, L.R., Hewitt, A.E., Webb, T.W., 2012. Soil and informatics science combine to develop S-map: a new generation soil information system for New Zealand. Geoderma 170, 232–238. https://doi.org/10.1016/j.geoderma.2011.11.012.
Lombardo, L., Opitz, T., Huser, R., 2018. Point process-based modeling of multiple debris flow landslides using INLA: an application to the 2009 Messina disaster. Stoch. Env. Res. Risk A. 32, 2179–2198.
Lombardo, L., Opitz, T., Ardizzone, F., Guzzetti, F., Huser, R., 2020. Space-time landslide predictive modelling. Earth-Sci. Rev. 209, 103318 https://doi.org/10.1016/j.earscirev.2020.103318.
Lombardo, L., Tanyas, H., Huser, R., Guzzetti, F., Castro-Camilo, D., 2021. Landslide size matters: a new data-driven, spatial prototype. Eng. Geol. 293 https://doi.org/10.1016/j.enggeo.2021.106288.
Lucía, A., Comiti, F., Borga, M., Cavalli, M., Marchi, L., 2015. Dynamics of large wood during a flash flood in two mountain catchments. Nat. Hazards Earth Syst. Sci. 15, 1741–1755. https://doi.org/10.5194/nhess-15-1741-2015.
Mackay-Smith, T.H., Burkitt, L., Reid, J., López, I.F., Phillips, C., 2021. A framework for reviewing silvopastoralism: a new Zealand Hill Country case study. Land 10, 1–28. https://doi.org/10.3390/land10121386.
Marden, M., Fuller, I.C., Herzig, A., Betts, H.D., 2018. Badass gullies: Fluvio-mass-movement gully complexes in New Zealand's East Coast region, and potential for remediation. Geomorphology 307, 12–23. https://doi.org/10.1016/j.geomorph.2017.11.012.
Martini, L., Cavalli, M., Picco, L., 2022. Predicting sediment connectivity in a mountain basin: a quantitative analysis of the Index of Connectivity. Earth Surf. Process. Landf. 1-14 https://doi.org/10.1002/esp.5331.
McDowell, R.W., 2014. Estimating the mitigation of anthropogenic loss of phosphorus in New Zealand grassland catchments. Sci. Total Environ. 468–469, 1178–1186.
McDowell, R.W., Schallenberg, M., Larned, S., 2018. A strategy for optimizing catchment management actions to stressor–response relationships in freshwaters. Ecosphere 9 (10), e02482. https://doi.org/10.1002/ecs2.2482.
Mondini, A.C., Guzzetti, F., Reichenbach, P., Rossi, M., Cardinali, M., Ardizzone, F., 2011. Semi-automatic recognition and mapping of rainfall induced shallow landslides using optical satellite images. Remote Sens. Environ. 115, 1743–1757. https://doi.org/10.1016/J.RSE.2011.03.006.
Moore, D.I., Burch, J.G., Mackenzie, H.D., 1988. Topographic Effects on the distribution of Surface Soil Water and the Location of Ephemeral Gullies. Trans. ASAE 31, 1098–1107. https://doi.org/10.13031/2013.30829.
Najafi, S., Dragovich, D., Heckmann, T., Sadeghi, S.H., 2021a. Sediment connectivity concepts and approaches. Catena 196, 104880. https://doi.org/10.1016/j.catena.2020.104880.
Najafi, S., Sadeghi, S.H., Heckmann, T., 2021b. Analysis of sediment accessibility and availability concepts based on sediment connectivity throughout a watershed. L. Degrad. Dev. 32, 3023–3044. https://doi.org/10.1002/ldr.3964.
New Zealand Government, 2020. National Policy Statement for Freshwater Management 2020. https://environment.govt.nz/publications/national-policy-statement-for-freshwater-management-2020/.
Page, M.J., Trustrum, N.A., Dymond, J.R., 1994. Sediment budget to assess the geomorphic effect of a cyclonic storm, New Zealand. Geomorphology 9, 169–188. https://doi.org/10.1016/0169-555X(94)90061-2.
Page, M.J., Reid, L.M., Lynn, I.H., 1999. Sediment production from Cyclone Bola landslides, Waipaoa Catchment. J. Hydrol. New Zealand 38 (2), 289–308.
Phillips, C., Hales, T., Smith, H., Basher, L., 2021. Shallow landslides and vegetation at the catchment scale: a perspective. Ecol. Eng. 173, 106436 https://doi.org/10.1016/j.ecoleng.2021.106436.
Poeppl, R.E., Dilly, L.A., Haselberger, S., Renschler, C.S., Baartman, J.E.M., 2019. Combining soil erosion modeling with connectivity analyses to assess lateral fine sediment input into agricultural streams. Water (Switzerland) 11. https://doi.org/10.3390/w11091793.
Preston, N.J., 2008. Off-slope sediment delivery from landsliding during a storm, muriwai hills, North Island. New Zealand IAHS-AISH Publ. 237–241.
Quinn, P.F., Beven, K.J., Chevallier, P., Planchon, O., 1991. The prediction of hillslope flow paths for distributed hydrological modelling using digital terrain models. Hydrol. Process. 5, 59–79.
R Core Team, 2021. R: A Language and Environment for Statistical Computing. R Foundation for Statistical Computing, Vienna, Austria.
Rahn, P.H., 2005. Geomorphology. In: Selley, R.C., Cocks, L.R.M., Plimer, I.R.B.T.-E. of G. (Eds.), Encylopedia of Geology. Elsevier, Oxford, pp. 90–95. https://doi.org/10.1016/B0-12-369396-9/00209-4.
Reid, L.M., Page, M.J., 2002. Magnitude and frequency of landsliding in a large New Zealand catchment. Geomorphology 49, 71–88. https://doi.org/10.1016/S0169-555X(02)00164-2.
Rickenmann, D., 1999. Empirical relationships for debris flows. Nat. Hazards 19, 47–77. https://doi.org/10.1023/A:1008064220727.
Rickenmann, D., 2005. Runout Prediction Methods, in: Debris-Flow Hazards and Related Phenomena. Springer, Berlin Heidelberg, pp. 305–324. https://doi.org/10.1007/3-540-27129-5_13.
Rigon, E., Comiti, F., Lenzi, M.A., 2012. Large wood storage in streams of the Eastern Italian Alps and the relevance of hillslope processes. Water Resour. Res. 48, 1–18. https://doi.org/10.1029/2010WR009854.
Riley, S.J., De Gloria, S.D., Elliot, R., 1999. A terrain ruggedness index that quantifies topographic heterogeneity. Int. J. Therm. Sci. 5, 23–27.
Rosser, B.J., Ross, C.W., 2011. Recovery of pasture production and soil properties on soil slip scars in erodible siltstone hill country, Wairarapa, New Zealand. New Zeal. J. Agric. Res. 54, 23–44. https://doi.org/10.1080/00288233.2010.535489.
Safari, S., Baratloo, A., Elfil, M., Negida, A., 2016. Evidence Based Emergency Medicine; Part 5 Receiver Operating Curve and Area under the Curve. Emerg. (Tehran, Iran), Vol. 4, pp. 111–113. https://doi.org/10.22037/emergency.v4i2.11903.
Sappington, J., Longshore, K., Thompson, D., 2007. Quantifying landscape ruggedness for animal habitat analysis: a case study using bighorn sheep in the Mojave Desert. J. Wildl. Manag. 71, 1419–1426.
Scheip, C., Wegmann, K., 2022. Insights on the growth and mobility of debris flows from repeat high-resolution lidar. Landslides. https://doi.org/10.1007/s10346-022-01862-2.
Simoni, S., Vignoli, G., Mazzorana, B., 2017. Enhancing sediment flux control and natural hazard risk mitigation through a structured conceptual planning approach. Geomorphology 291, 159–173. https://doi.org/10.1016/j.geomorph.2017.01.026.
Smith, H.G., Spiekermann, R., Betts, H., Neverman, A.J., 2021. Comparing methods of landslide data acquisition and susceptibility modelling: examples from New Zealand. Geomorphology 107660. https://doi.org/10.1016/j.geomorph.2021.107660.
Spiekermann, R.I., McColl, S., Fuller, I., Dymond, J., Burkitt, L., Smith, H.G., 2021. Quantifying the influence of individual trees on slope stability at landscape scale. J. Environ. Manag. 286, 112194 https://doi.org/10.1016/j.jenvman.2021.112194.
Spiekermann, R.I., Smith, H.G., McColl, S., Burkitt, L., Fuller, I.C., 2022. Quantifying effectiveness of trees for landslide erosion control. Geomorphology 396, 107993. https://doi.org/10.1016/j.geomorph.2021.107993.
Storey, R., Wadhwa, S., 2009. An Assessment of the Lengths of Permanent, Intermittent and Ephemeral Streams in the Auckland Region. Auckl Reg. Counc. Tech. Rep. 0504.
Thompson, R.C., Luckman, P.G., 1993. Performance of biological erosion control in New Zealand soft rock hill terrain. Agrofor. Syst. 21, 191–211. https://doi.org/10.1007/BF00705230.
Tibshirani, R., 1996. Regression Shrinkage and selection via the Lasso. J. R. Stat. Soc. Ser. B Methodol. 58 (1), 267–288.
Wall, A.J., Mackay, A.D., Kemp, P.D., Gillingham, A.G., Edwards, W.R.N., 1997. A review of the impacts of widely spaced soil conservation trees on hill pastoral systems. Proc. New Zealand Grassland Assoc. 59, 171–177.
Wang, L., Liu, H., 2006. An efficient method for identifying and filling surface depressions in digital elevation models for hydrologic analysis and modelling. Int. J. Geogr. Inf. Sci. 20, 193–213.
Wichmann, V., Heckmann, T., Haas, F., Becht, M., 2009. A new modelling approach to delineate the spatial extent of alpine sediment cascades. Geomorphology 111, 70–78. https://doi.org/10.1016/j.geomorph.2008.04.028.
Xiong, J., Tang, C., Gong, L., Chen, M., Li, N., Shi, Q., Zhang, X., Chang, M., Li, M., 2022. How landslide sediments are transferred out of an alpine basin: evidence from the epicentre of the Wenchuan earthquake. Catena 208, 105781. https://doi.org/10.1016/j.catena.2021.105781.
Zevenbergen, L.W., Thorne, C., 1987. Quantitative analysis of land surface topography. Earth Surf. Process. Landf. 12, 47–56.
Zhao, G., Gao, P., Tian, P., Sun, W., Hu, J., Mu, X., 2020. Assessing sediment connectivity and soil erosion by water in a representative catchment on the Loess Plateau. China Catena 185, 104284. https://doi.org/10.1016/j.catena.2019.104284.
Ziemer, R.R., Lewis, J., Rice, R.M., Lisle, T.E., 1991. Modeling the cumulative watershed effects of forest management strategies. J. Environ. Qual. 20, 36–42. https://doi.org/10.2134/jeq1991.00472425002000010008x.